International Journal of Greenhouse Gas Control 115 (2022) 103591

Contents lists available at ScienceDirect

International Journal of Greenhouse Gas Control

journal homepage: www.elsevier.com/locate/ijggc

# Techno-economic optimization and off-design analysis of $CO_2$ purification units for cement plants with oxyfuel-based $CO_2$ capture

Francesco Magli [a,b], Maurizio Spinelli [c], Martina Fantini [c], Matteo Carmelo Romano [a], Manuele Gatti [a,*]

[a] Politecnico di Milano, Department of Energy, via Lambruschini 4, 20156 Milan, Italy
[b] Buzzi Unicem SpA, via Luigi Buzzi 6, 15033 Casale Monferrato, Italy
[c] Laboratorio Energia e Ambiente Piacenza (LEAP), via Nino Bixio 27/C, 29121 Piacenza, Italy

ARTICLE INFO

*Keywords:*
$CO_2$ purification unit
$CO_2$ capture
Oxyfuel
Calcium looping
Cement decarbonization

ABSTRACT

This paper evaluates the technical and economic performance, as well as the direct/indirect $CO_2$ emissions of the $CO_2$ Purification Unit (CPU) for cement plants equipped with oxyfuel-based $CO_2$ capture. Two configurations, targeting two different outlet $CO_2$ specifications ('moderate' 95% purity and 'high' 99.9% purity) are designed, modelled and optimized in order to minimize the incremental clinker production cost for different values of the carbon tax. Mass and energy balances are simulated with Aspen Plus, while the operating conditions are numerically optimized with Matlab. Results show that moderate purity can be achieved with an increased cost of clinker of 16.3 €/$t_{clk}$ ($CO_2$ recovery 99.3%), while the base high purity configuration leads to a 19.3 €/$t_{clk}$ increase ($CO_2$ recovery 96.1%). Sensitivity analyses are carried out on design parameters (fuel and air infiltrations in the oxyfuel calciner line) and exogenous factors (carbon tax, $CO_2$ intensity of electricity). Air infiltration rate has the highest impact on the incremental cost of clinker (increased by 25% when air leakage grows from 0 to 10%) and on the selection of optimal operational conditions. Off-design analyses aimed at assessing the impact of air infiltration changing over time highlight the relevance of designing the CPU for the scenario with air infiltrations, while selecting reasonable temperature differences (e.g. 5K) to avoid operability issues in the cold box heat exchanger. For the base case CPU, the cost of clinker increases by 3 €/$t_{clk}$ when moving from zero to 10% air infiltration.

## 1. Introduction and goals

$CO_2$ Capture Utilisation and Storage (CCUS) technologies are increasingly seen as an essential mitigation strategy required to meet the decarbonization goals on a worldwide basis in key industrial sectors such as industry (cement, steel, refineries, blue hydrogen, etc.) and power generation (IEA, 2020).

Together with post-combustion and pre-combustion, oxyfuel processes are among the possible pathways for $CO_2$ capture (Bui et al., 2018) (Leung et al., 2014). Compared to the alternative techniques, the key advantage of oxyfuel is the removal of nitrogen from the oxidant which would otherwise act both as a thermal "ballast", as a possible origin of thermal NOx emissions and as a $CO_2$ dilutant in the exhaust gas stream, therefore making its separation more energy-intensive and expensive (Bui et al., 2018), (Seddighi et al., 2018). By contrast, oxy-combustion typically envisages as a major drawback, in terms of energy penalty and costs, the need of an Air Separation Unit (ASU), required to supply nearly pure oxygen as oxidant stream (typical purities envisaged in oxyfuel processes ranging between 95% and 99.5%, depending on the specific application (Kim et al., 2012), (Nemitallah et al., 2017), (Scaccabarozzi et al., 2016). Besides the ASU, the second most significant "auxiliary" unit of oxyfuel $CO_2$ capture technologies is the $CO_2$ Purification Unit (CPU), whose impact from the point of view of thermodynamic performance and costs is often underrated. A proper design of the CPU for oxyfuel-based capture plants is crucial not only to ensure that the capture unit produces a $CO_2$ stream meeting the technical specifications required by the subsequent transportation and utilization/storage steps of the CCUS value chain, but also because the performance and costs of the CPU itself may have a significant impact on the viability and competitiveness of the whole CCUS project. The importance of the CPU for the competitiveness of oxyfuel technologies is demonstrated not only by the several modelling works (e.g. (Kolster et al., 2017) and (Xu et al., 2021)) aiming at identifying alternative,

* Corresponding author.
*E-mail address:* manuele.gatti@polimi.it (M. Gatti).

https://doi.org/10.1016/j.ijggc.2022.103591
Received 14 May 2021; Received in revised form 31 December 2021; Accepted 19 January 2022
Available online 24 February 2022
1750-5836/© 2022 The Authors. Published by Elsevier Ltd. This is an open access article under the CC BY-NC-ND license (http://creativecommons.org/licenses/by-nc-nd/4.0/).

**Nomenclature**

*Acronyms*

| | |
|---|---|
| ASU | Air Separation Unit |
| CaL | Calcium Looping |
| CAPEX | CAPital EXpenditure |
| CCR | Capital Charge Rate |
| CCS | $CO_2$ Capture and Storage |
| CCUS | $CO_2$ Capture Utilisation and Storage |
| CLEANKER | CLEAN clinKER production by calcium looping process |
| CPU | $CO_2$ Purification Unit |
| CRR | $CO_2$ Recovery Ratio |
| CT | Carbon Tax |
| ECBM | Enhanced Coal Bed Methane |
| ECRA | European Cement Research Academy |
| EOR | Enhanced Oil Recovery |
| ESDU | Engineering Sciences Data Unit |
| GPDC | Generalized Pressure Drop Correlation |
| HEX | Heat Exchanger |
| IEA | International Energy Agency |
| IPCC | Intergovernmental Panel on Climate Change |
| KPI(s) | Key Performance Indicator(s) |
| MITA | Minimum Temperature Approach |
| OPEX | OPerating Expense |
| PFHE | Plate-Fin Heat Exchangers |
| ppm | part per million |
| ppmv | part per million – volume fraction |
| RDF | Refuse Derived Fuel |
| RES | Renewable Energy Sources |
| SPECCA | Specific Primary Energy Consumption for CO2 Avoided |
| TEA | Techno-Economic Assessment |
| TPC | Total Plant Cost |
| tpd | tonne (metric ton) per day |
| TSA | Temperature Swing Adsorption |
| TRL | Technology Readiness Level |

*Symbols*

| | |
|---|---|
| $\beta$ | compression ratio |
| $\beta_i$ | volumetric heat transfer coefficient for stream $i$ |
| $\beta_z$ | volumetric heat transfer coefficient for zone $z$ |
| $c_i$ | cost of element i |
| clk | clinker |
| $\Delta T_{m,z}$ | zonal logarithmic mean temperature difference |
| $e_{CO_2,d}$ | direct $CO_2$ specific emissions |
| $e_{CO_2,eq}$ | equivalent $CO_2$ specific emissions |
| $e_{CO_2,ind}$ | indirect $CO_2$ specific emissions |
| $k_{ij}$ | binary interaction parameters |
| $\dot{m}$ | mass flow rate |
| Ndes | design rotational speed |
| $P_{el}$ | specific electric consumption |
| $\dot{Q}_z$ | total heat transferred in zone $z$ |
| $\dot{Q}_i$ | heat transferred by the $i$-th of the $n$ streams involved in zone $z$ |
| U•A | product between the overall heat transfer coefficient and the heat transfer area |
| $V_z$ | zonal volume |
| $\dot{W}$ | Electric power |

more efficient and optimized schemes, but also by the construction and testing for several thousands of operational hours of dedicated pilots at relevant scale (Lockwood, 2014), such as CIUDEN (Delgado et al., 2014), Callide (Komaki et al., 2014) and Schwarze Pumpe (White et al., 2013) pilots. These pilot plants were all TRL-7 units, processing flue gases from coal-fired oxyfuel boilers, with capacities ranging from 10 to 240 $t_{CO2}$/d (Lockwood, 2014), (Delgado et al., 2014), (Spero and Yamada, 2018), (Burchhard and Griebe, 2013). The demonstrators, as well as most of the literature on the CPU, target the application to oxy-fired power plants, while this work focuses on oxyfuel-based capture in cement plants.

In cement plants, most of $CO_2$ emissions derive from the calcination process. More specifically, in state-of-the-art plants based on dry process with pre-calciner and solid fuels, around 60% of the total $CO_2$ derive from $CaCO_3$ decomposition, 20–25% derive from the fuel burned in the pre-calciner and 15–20% from the fuel burned in the rotary kiln. In these plants, oxyfuel calcination is particularly competitive because a given amount of high purity oxygen (i.e. with a given cost associated to $O_2$ production) allows capturing a higher amount of $CO_2$ compared to conventional combustion processes (not only the $CO_2$ from fuel combustion but also the $CO_2$ from $CaCO_3$ calcination). As a consequence, the lowest Specific Primary Energy Consumption for $CO_2$ Avoided (SPECCA) and the lowest cost of $CO_2$ avoided have been predicted for oxyfuel-based technologies among a range of alternative CCS options, including post-combustion solvent-based scrubbing (Voldsund et al., 2019), (Gardarsdottir et al., 2019a). The following most interesting oxyfuel processes for the cement sector can be listed (IEAGHG, 2013a), (Hills et al., 2016):

- Full oxyfuel (European Cement Research Academy, 2016), (Carrasco-Maldonado et al., 2016), where both the kiln and the calciner of the clinker production plant use oxygen in place of air to fully decarbonise cement production.
- Partial oxyfuel (De Lena et al., 2021), (Gimenez et al., 2014), where only the calciner is oxyfired, renouncing to capturing the $CO_2$ generated in the rotary kiln, but avoiding dealing with the costs and technological risks related to the conversion of the rotary kiln into oxyfuel and of the clinker cooler from air-cooled to $CO_2$-cooled system.
- Calcium looping (CaL), especially the integrated configuration (De Lena et al., 2019), where the CaL calciner fully replaces and integrates the usual cement plant pre-calciner.

A common feature of the three aforementioned oxyfuel processes for cement is not only the oxyfuel calcination arrangement, but also the requirement of a CPU, where the $CO_2$ is conditioned, purified and compressed until the dense/liquid phase, to meet the quality specifications for transport and storage.

This work originates from CLEANKER (www.cleanker.eu, 2021), an EU-funded H2020 R&D project, which aims at demonstrating at TRL-7 (i.e. demonstration in relevant operational environment) the integrated CaL technology, via the construction and operation of a first-of-a-kind pilot plant in a commercial-scale cement plant located in Vernasca (Italy). Given its impact on performance and cost of $CO_2$ avoided, the CPU is an essential unit of the integrated CaL process, whose assessment and optimization is required to fully validate the techno-economic viability of low-carbon cement plants based on oxyfuel calcination. Therefore, achieving an efficient and cost-optimized CPU design is crucial to the technical and economic success of the overall CCUS chain. In CLEANKER, the technical, environmental and economic performance of different CPU configurations for the full-scale integrated Calcium Looping cement plant are evaluated with process simulations and techno-economic assessments (Magli et al., 2019). This work presents the methodology, design and off-design results from the numerical process optimization of two CPU configurations, with case studies tailored to the $CO_2$-rich mixture produced by a full-scale integrated CaL

plant, and designed for two different quality specifications of the $CO_2$ final product.

In literature, the vast majority of the papers dealing with CPU target its application to oxy-fuel power plants, for which modelling and techno-economic evaluations for different configurations and range of purities are reported, while only a limited number of papers are focused on the CPU for cement plants. Among the power plant related CPUs, (Kolster et al., 2017) modelled different CPU configurations, including distillation, for coal-fired oxyfuel power-plants and they studied the trade-off between $CO_2$ purity and costs for the optimization of the $CO_2$ transport network located in UK; (Porter et al., 2017) evaluated KPIs and costs for the same three alternative CPU options from Kolster but at fixed design conditions and without techno-economic optimization; (Jin et al., 2015) carried out a thermodynamic optimization and dynamic analysis for a flash-based CPU of an oxyfuel power plant to identify the control strategy in case of load or flue gas composition change, however focusing on process performance only and without assessing the costs.

Concerning the CPU application to cement CCUS, the works by (IEAGHG, 2013a), (Atsonios et al. (2015), (Rolfe et al., 2018) and (Voldsund et al., 2019) are relevant. The IEAGHG report on CCUS deployment in the cement industry (IEAGHG, 2013a) discusses the impact of the CPU on the overall capture rate of both full and partial oxyfuel technologies, highlighting that, depending on air leakages and CPU technology, the $CO_2$ capture rate for full oxyfuel could be in the range 85–99%, while the partial oxyfuel allows nearly 60–70% capture. Moreover, the report estimates the CPU electric consumption to be comparable with the electric demand of the whole reference cement plant without capture in the full oxyfuel case, or half of that in the partial oxyfuel capture, and it also underlines the role of false air ingress on CPU performance in terms of flow rate and efficiency changes.

Atsonios et al. (2015) carried out a techno-economic assessment of tail-end calcium looping integration in an existing cement plant, including the simulation of a low-temperature CPU based on a distillation column operating close to the $CO_2$ triple point (5 bar reported in the paper) with externally refrigerated top condenser. In their assessment, process conditions are fixed, the capital cost is estimated as a lump-sum and it is reported that a change in the oxygen excess should not affect the electric consumption of the CPU.

Rolfe et al. (2018) performed a technical and environmental assessment of tail-end CaL and oxy-fuel for cement decarbonization. Both processes, despite achieving different $CO_2$ capture rates (94% for CaL, close to 100% for the full oxyfuel process), include a downstream double-flash-based CPU (similar to the “moderate purity” case from the present paper) and air infiltration is assumed in the preheater and kiln (0.33 kg of additional air/kg of clinker). In both cases the CPU is the largest unit in terms of power consumption, featuring a non-negligible impact on the plant overall power demand (close to 42%, with a specific consumption of 134 kWh/$t_{CO2}$ in CaL and 154 kWh/$t_{CO2}$ in full oxyfuel), however no details are reported on the process conditions selected for the CPU and no economic, nor off-design analysis is reported.

The CEMCAP (http://www.sintef.no/cemcap/, H2020 project, GA 641,185) consortium (Voldsund et al., 2019) assessed the techno-economic analysis of the following oxy-fuel based processes: (i) full-oxyfuel, (ii) tail-end CaL, (iii) integrated CaL, for a given final $CO_2$ purity (targeting >95% $CO_2$, hence in line with the “moderate purity” case from this paper) and for a fixed CPU scheme, designed as a single stage flash self-refrigerated unit. The paper by (Voldsund et al., 2019), then completed by the economic results by (Gardarsdottir et al., 2019a) where sizing and costing is detailed at the equipment-level for the whole process including the CPU, assumes given process conditions (discussed in (Jamali et al., 2018) which highlights the trade-off between $CO_2$ capture ratio and purity in the CPU), reports very similar CPU consumptions close to 120 kWh/$t_{CO2}$ for all the three oxyfuel processes, while it does not carry out a numerical optimization, nor covering off-design analysis.

The present paper is therefore a first contribution assessing the optimal design of the CPU applicable to oxyfuel-based calcination from a techno-economic stand-point, with case studies accounting for off-design and sensitivity analysis on the impact of parameters relevant to the application of integrated CaL. Two full-scale CPU configurations are defined and described in section 2: moderate purity based on two stage flash separation and high purity based on a $CO_2$ distillation column.

More in detail, the novel contributions from this work are:

1 Techno-economic numerical optimization of the CPU, aimed at finding via automatic process simulations, sizing and costing, the design conditions which minimize the incremental cost of clinker due to the CPU;
2 Sensitivity analyses to evaluate how process design parameters (fuel burnt, oxygen excess and air infiltrations in the calciner) and exogenous parameters (carbon tax, $CO_2$ intensity of electricity generation) affect the optimal design, the thermodynamic performance and the costs of the CPU;
3 Off-design evaluation to assess the impact of increasing air infiltrations in the oxyfuel calciner section over time, between two scheduled maintenance periods;
4 Identification of design criteria for the full-scale CPU of oxyfuel-based cement plants.

The paper is structured as follows: section 2 describes the CPU process configurations considered together with the $CO_2$ technical specifications required to cope with the transportation and storage requirements. Section 3 reports the methodology employed for the design of the CPU and the techno-economic optimization at nominal (i.e. full-load conditions); while section 3.1 pinpoints the case studies analysed, section 3.2 illustrates the basis of design with all the technical assumptions, section 3.3 summarizes the energy performance and cost results for the optimal points and section 3.4 reports a sensitivity analysis on the most significant parameters affecting the CPU design. Section 4 is devoted to the off-design analysis required to deal with the air infiltrations from the calciner shared by the cement and $CO_2$ capture plants. Section 5 identifies the key CPU technical guidelines resulting from the design and off-design optimisations and techno-economic analyses. Section 6 draws the conclusions of the research.

## 2. $CO_2$ Purification Unit (CPU): process configurations

Although this study presents the results related to the application of an optimized CPU to the integrated CaL process, the scheme has a general validity for cement plants equipped with oxyfuel-based $CO_2$ capture requiring a CPU.

The main plant subsections included in the CPU are the following: a dust abatement step based on a fabric filter in order to protect the downstream equipment; a first compression step with water condensation after inter-cooling and removal by means of knock-out drums; a dehydration step based on solid bed adsorption (thermally regenerated) for the further reduction of the water content down to the ppm-design specification; the main cold box entailing low temperature multiflow heat exchangers, phase separators and columns (where required); a final step of inter-cooled compression and final pumping of the purified $CO_2$ in the dense-phase to 110 bar. Other pre-treatment steps located ahead of the CPU may be required depending on the specific fuel adopted and operational conditions of the oxyfuel calciner. Therefore, as described by dedicated papers (Shah et al., 2011) and (Besong et al., 2013), activated carbon bed, permanganate towers or other scrubbing systems for NOx and SOx control or guard beds for other minor impurities or trace elements could be included depending on the specific amounts of contaminants to be removed. However, their presence would not affect the design and optimization of the CPU.

The process flow diagram of the “Moderate Purity” CPU is depicted in Fig. 1, while the one for the “High Purity” CPU is shown in Fig. 2.

While the two configurations described in the following are kept fixed throughout this study, the operating conditions (i.e. temperature, pressures, etc.) are not reported in the scheme description of this section, since they are optimized on a case-by-case scenario as described in section 3.

The Moderate purity configuration (Fig. 1) replicates the one proposed by IEAGHG (IEAGHG, 2011) for the purification of flue gases produced by a coal-fired oxyfuel boiler: at the exit of the bag filter, a blower overcomes the pressure drops across the calciner and dust filter connections to produce a depulverized raw $CO_2$ stream #3 ready for compression in multi-stage intercooled compressor-1 (configured as from the 'Oxy-fuel – Optimized inter-cooling as specified' scheme presented by (IEAGHG, 2011)), then stream #4 is further compressed until the operating pressure of the dehydration unit, which produces a fully dehydrated stream #8, ready to be purified and partly condensed in the cold box. The stream recycled between the adsorption-based dehydration unit and the inlet of compressor-2 is dried $CO_2$ used for the adsorption bed regeneration. The fraction, 10% of the total $CO_2$ stream #8, is set according to state-of-the-art values reported by (IEAGHG, 2011). The cold box includes a double flash separation process where the $CO_2$ is cooled down at low temperatures (minimum values close to −50°C) and partly liquefied and separated in two sequential steps (Heat Exchanger-1, Separator-1 and Heat Exchanger-2 and Separator-2), at near constant pressure (except for pressure drops). $CO_2$ purification occurs during phase separation, as a result of the volatility difference between $CO_2$ and other mixture components, i.e. $O_2$, $N_2$ and Ar, the liquid phase (streams #22 and #17), leading to a liquid stream richer in $CO_2$ and to a gaseous stream containing most of the non-condensable species (stream #12). The scheme is auto-refrigerated, since the cooling duty required is provided directly via throttling the $CO_2$-rich liquid streams #22 and #18, which are then heated while cooling down the raw $CO_2$ mixture in countercurrent and leave the Heat Exchanger-1 fully vaporized as streams # 24 and #21. These streams, coping with the composition specifications required for moderate purity $CO_2$, are finally compressed up to 110 bar via a three stage inline intercooled compressor followed by a pump and cooled to 30°C in an aftercooler. The produced liquid $CO_2$ stream #$CO_2$-110 leaves the boundary limits of the cement plant for the subsequent transportation, utilization and storage steps of the CCUS value chain. Vapor stream #12 recovers cooling duty for auto-refrigeration purposes by crossing Heat Exchangers-1 and 2 in countercurrent with respect to the raw $CO_2$ mixture.

The High Purity scheme (Fig. 2) is based on the process configuration patented by Air Products (White and Allam, 2008), in the version presented by Strube and Manfrida (Strube and Manfrida, 2011). The dust abatement, compression and dehydration sections are the same as from the moderate purity case (however, the pressure may change due to optimization), while the cold box includes a single multi-stream heat exchanger, featuring two hot streams (#9 and #11) and five cold streams (#13, #18, #20, #26, #28), followed by a flash separator and a stripping column with a reboiler. Stream #9 enters the low temperature heat exchanger where it is pre-cooled, then it goes into the hot side of the reboiler, where it is further cooled while providing the heat duty required to attain the specified content of $O_2$ in the final $CO_2$ product (i.e. 10 ppmv $O_2$) and it is eventually cooled down to the minimum temperature selected to produce (i) a $CO_2$-rich liquid stream #13, and (ii) a $CO_2$-lean and non-condensables-rich vapour (stream #26) which is vented after refrigeration power recovery. Stream #13 is partly vaporized in order to provide auto-refrigeration for the hot streams and then throttled before entering the stripper from the top stage. The stripper, configured as a countercurrent packed column with a reboiler at the bottom, produces the purified $CO_2$ product #16 as saturated liquid and a saturated vapor #28 from the top which is recompressed and mixed as stream #31 with the inlet raw $CO_2$ #8 to minimize the $CO_2$ losses. The column has no overhead condenser, since the recycle #31 with the separator and related cold box section act as a top condenser (with cooling, partial condensation, separation and recycle of the vapor stream exiting from the top of the column). Valve-2 and 3 and the upstream splitter operate to provide the required auto-refrigeration duty to cool down streams #9 and #11; as a result, streams #21 and #24 are fully vaporized, although at different pressures. The final compressors-3 and 4 and $CO_2$ pump are arranged as in the Moderate Purity scheme.

The Moderate and High Purity schemes share the following features: (i) the non-condensable rich stream leaving the CPU (#14 in the moderate purity case and #27 in the high purity case) is assumed to be vented, even though additional $CO_2$ recovery technologies, based on different separation principles, may be installed downstream the low-temperature CPU to recover these $CO_2$ which is otherwise emitted. The possible options are: adsorption on solid materials (P/TSA, Pressure/Temperature Swing Adsorption) (Shah et al., 2011), membrane separation (White et al., 2006), or recycle to the CaL carbonator reactor (De Lena et al., 2017), (Romano, 2013). (ii) In both schemes, no expanders are placed on the vapor branch leaving the phase separator, because according to the preliminary analysis they would have a small size even in the full-scale plant, since they could generate a few hundred kilowatts of electricity (the maximum theoretical production with a two-stage isentropic expander in the moderate case is between 400 and 500 kW) and a similar amount of low temperature cooling duty, resulting in a limited impact on the energy performance of the CPU.

### 2.1. $CO_2$ quality specifications

The outlet specifications for the CPU depend both on the transportation system and on the final destination of the captured and purified $CO_2$.

The considered transportation options are:

- Pipeline: it is a known and mature market technology, with significant experience from more than 8'200 km of $CO_2$ pipelines in the United States (as of 2019) (Pipeline and Hazardous Materials Safety Administration, 2021). There is also some experience with transport of $CO_2$ using offshore pipelines (around 150 km) in Snøhvit, Norway (International Energy Agency, 2013), (IEAGHG, 2013b);
- Shipping: it may be economically attractive when the $CO_2$ has to be moved over large distances or overseas in small quantities. The largest ships for $CO_2$ transport are in the 8'500 – 10'000 $m^3$ range (6 ships of this size were in operation worldwide in 2010, according to Energy Institute, 2010). However, new ships are currently under design to address the specific CCS demands, hence carriers with capacity up to 30'000 – 40'000 $m^3$ could become economically feasible. It has to be noticed that a ship-based transportation system must include, unlike a pipeline-based system, temporary storage on land and a loading facility (IPCC, 2005), (Energy Institute, 2010), (IEAGHG, 2020).

Other options, such as road and rail tankers are also technically feasible, but they are uneconomical except on a very small scale (IPCC, 2005), hence they are not interesting for full-scale CCS projects in the field of cement.

A literature survey has been carried out to have an overview of the specifications which has been considered in research projects, national and international standards and actual transport/storage projects. The results of this review – limited to the contaminants specifically relevant for the current work – are reported in the Supplementary material of this work.

Based on this review, two $CO_2$ quality specifications have been defined, considering two extreme (yet reasonable) conditions:

- Moderate purity: this option considers the transport and storage system which features the least strict specifications. It is representative of a pipeline transport system operated in a hot region and storage in a deep saline formation. The 'moderate purity' case is based on the least strict limits set by the European standards for $CO_2$

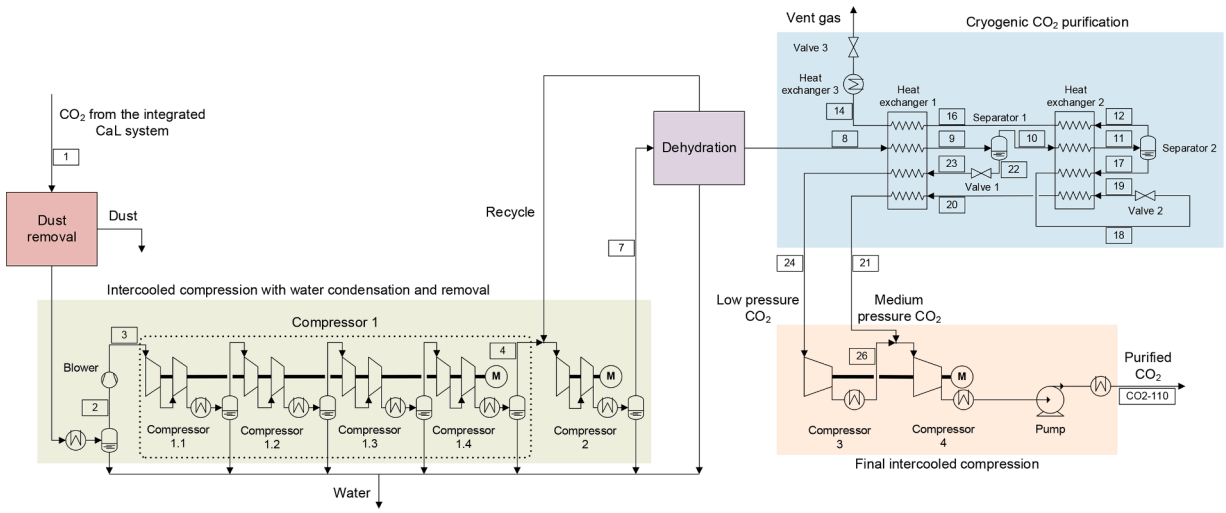


**Fig. 1.** Process flow diagram and plant boundaries of the Moderate Purity CPU.

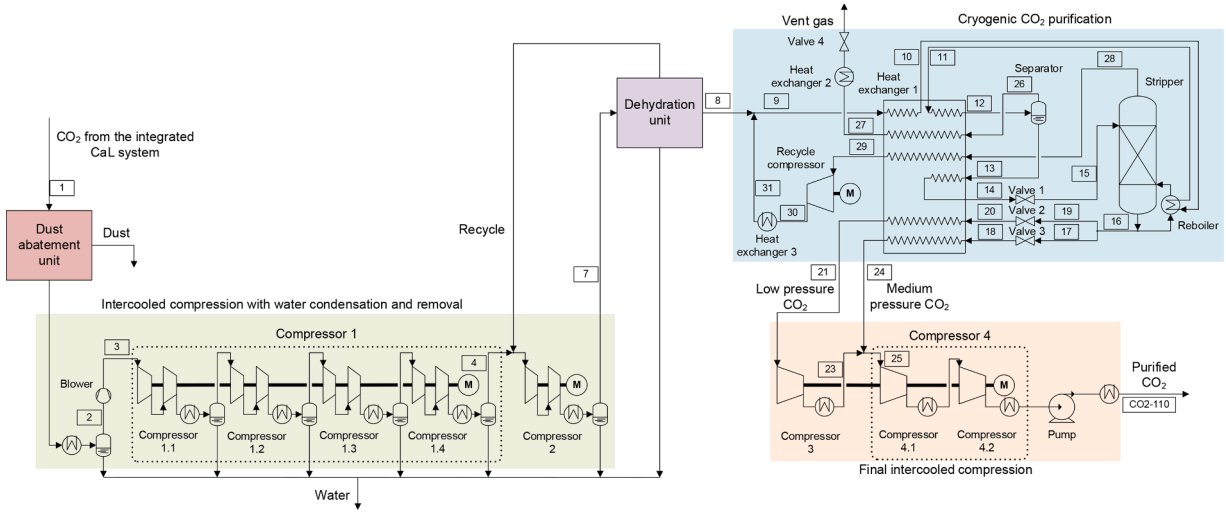


**Fig. 2.** Process flow diagram and plant boundaries of the High Purity CPU.

pipelines (ISO 27,913, 2016), under the assumption that no further limitations are given by the storage site. The content of particulates is limited as suggested by the Teesside CCS Project (AMEC, 2015);

- High purity: on the opposite side, this option considers the most severe specifications that a $CO_2$ transport and storage system (not deemed for food applications) can require. It is representative of a multi-modal transport system featuring both pipeline and ship transport, located in a cold region (e.g. Northern Europe or Canada) and with final utilization of the $CO_2$ for EOR. Pressure and temperature are imposed by the pipeline operation, while the presence of impurities (in particular, non-condensable gases) is limited by the ship transport conditions. An additional limitation on the oxygen content is due to microbial related corrosion which may affect the pipeline in terms of corrosion, as well as injection wells, particularly for EOR (Bliss et al., 2010). The 'high purity' case is mainly based on the specifications for ship transport suggested in (Maroto-Valer, 2010), while limitations on $SO_2$, NOx and particulates content are kept identical to the 'moderate purity' option.

In both cases, the water content is limited by the CPU, so it is not dependent on the subsequent transport/storage options: low-temperature heat exchangers operate close to the triple point of $CO_2$ (−56.6°C), hence deep dehydration is required in order to prevent the formation of ice (Berstad and Trædal, 2018).

The $CO_2$ quality specifications for the two options selected in this paper are reported in Table 1, where also the concentrations of two relevant full-scale $CO_2$ storage projects are reported (i.e. Northern Lights and the Teesside project).

## 3. Techno-economic optimization under design conditions: methodology

The problem tackled in this paper involves the simultaneous design, sizing and cost evaluation of two configurations of the $CO_2$ Purification Unit (CPU) for moderate and high $CO_2$ purity specifications, applied to a 3000 tpd cement plant equipped with integrated CaL system. The numerical optimization problem of such a system involves the following steps, outlined in Fig. 3:

1 For each selected CPU case study and for given design conditions (key pressures, temperatures and split fractions), the process flowsheet is simulated with Aspen Plus v10, mass and heat balances are solved and the $CO_2$ recovery efficiency and energy performance can be computed.
2 Simulation results are transferred to ad hoc Matlab functions aimed at carrying out the sizing and costing of each equipment unit (i.e.

**Table 1**
Assumed $CO_2$ specifications and comparison with Teesside and Northern Lights project specifications. Where '-' is reported, the specification on the 'Total' amount applies.

| | | | Moderate purity (this work) | High purity (this work) | *Teesside project* (Brownsort, 2019) | *Northern Lights project* (Fortum Oslo Varme AS, 2020) |
|---|---|---|---|---|---|---|
| Pressure | | bar(a) | 110 | 110 | - | - |
| Temperature | | °C | 30 | 30 | - | - |
| Composition | | | | | | |
| $CO_2$ | | vol% (min) | 95 | 99.7 | *95* | - |
| $H_2O$ | | ppmv | 1 | 1 | *50* | *30* |
| Non condensables | $N_2$ | vol% | 2 | - | *1* | - |
| | $O_2$ | ppmv | - | 10 | *10* | *10* |
| | Ar | vol% | - | - | *1* | - |
| | $CH_4$ | vol% | - | - | *1* | - |
| | $H_2$ | vol% | 0.75 | - | *1* | *0.005* |
| | CO | vol% | 0.2 | 0.2 | *0.2* | *0.01* |
| | Total | vol% | 4 | 0.3 | - | - |
| $H_2S$ | | ppmv | 200 | 200 | *200* | *9* |
| $SO_2$ | | ppmv | 50 | 50 | *100* | *10* |
| NOx | | ppmv | 50 | 50 | *100* | *10* |
| Particulates | | mg/Nm$^3$ | 1 | 1 | *1* | - |

calculate compressor capital cost, heat exchangers area and capital cost, electricity cost, $CO_2$ emissions, etc.) and complete the economic assessment.

3 The objective function is computed, namely the incremental cost of clinker (due to the presence and operation of the CPU), $\Delta c_{clk,CPU}\left[\frac{€}{t_{clk}}\right]$, calculated as from eq. (1):

$$\Delta c_{clk,CPU} = \frac{TPC_{CPU}\cdot CCR}{clk_{prod}} + CO2_{tax} + OPEX_{el,\ CPU} + OPEX_{wat,\ CPU} + OPEX_{FIXED,\ CPU} \quad (1)$$

which includes the following contributions per ton of decarbonized clinker produced: the CPU capital cost ($TPC_{CPU}$) multiplied by the capital carrying charge rate (CCR), which depends on the financial assumptions discussed further on), and divided by the yearly clinker production rate ($clk_{prod}$, expressed in $t_{clk}$/y), the CPU variable operating costs for electricity purchase ($OPEX_{el,\ CPU}$) and for cooling water ($OPEX_{wat,\ CPU}$), the $CO_2$ emissions cost ($CO2_{tax}$) due to carbon tax on both direct (i.e. Scope 1, $CO_2$ emitted from the plant stack) and indirect (i.e. Scope 2, $CO_2$ emitted due to the import of electricity) emissions, and the CPU fixed operating costs $OPEX_{FIXED,\ CPU}$ (i.e. fixed maintenance and insurance). Details on the calculation of the TPC are reported in the Supplementary material.

After step 3, the objective function value is returned to the numerical optimizer, which is the Matlab R2019b particle swarm solver for derivative-free optimization with bounds on the decision variables, which is based on the algorithm presented by (Kennedy and Eberhart, 1995), as modified by (Mezura-Montes and Coello Coello, 2011) and (Pedersen, 2010). A swarm size of 50 is used and the maximum number of iterations after which the optimizer automatically stops is set to 2000. The optimizer automatically changes the design conditions targeting a lower $\boldsymbol{\Delta c_{clk,CPU}}$ cost until max number of iterations (2000 per each case) or convergence is reached. For each iteration, this step by step procedure (simulation, performance and cost calculation, objective function computation) is repeated.

Section 3.1 describes the methods and assumptions adopted for the CPU process design, modelling and simulation, while section 3.2 the definition of the Key Performance Indicators (KPIs) for performance, emissions and cost assessment. Paragraph 3.3 identifies the case studies, starting from the base case and highlighting the parameters changed in the sensitivity. In paragraph 3.4 the optimization results are presented and discussed for the base case, while paragraph 3.5 reports the results of the sensitivity analysis.

### 3.1. Process modelling and simulation

Energy and mass balances at steady state are calculated with Aspen Plus v10 (AspenTech, 2019), using the sequential modular process simulation approach. The thermo-physical properties of the fluid mixtures are modelled with the cubic Peng-Robinson equation of state with classical Van der Waals mixing rules, with the following values for the binary interaction parameters $k_{ij}$:

- $k_{CO2—O2} = 0.114$ (Li and Yan, 2009)
- $k_{CO2\text{-}Ar} = 0.163$ (Li and Yan, 2009)
- $k_{CO2—N2} = -0.017$ (Aspen Plus, default for PENG-ROB from APV100 EOS-LIT databank)
- $k_{CO2—H2O} = 0.12$ (Aspen Plus, default for PENG-ROB from APV100 EOS-LIT databank)

Other EOS can be used to simulate this process, such as the GERG-2008 model (Kunz and Wagner, 2012), however the selected Peng-Robinson model provides a reasonable compromise between accuracy and calculation speed.

The most significant process design assumptions are described in the following or listed in Table 2, while other assumptions are reported in the Supplementary material.

Concerning the equipment sizing, the following methodology has been employed:

- Compressors efficiency differ for each group, and even on a stage-by-stage basis for compressor-1, due to the different volumetric flow rates elaborated. The assumed polytropic efficiency values are representative of large-scale CO2 centrifugal compressors and they have been taken from (IEAGHG, 2011). In multi-stage machines, overall compression ratios have been split equally (constant beta rule) among the stages.

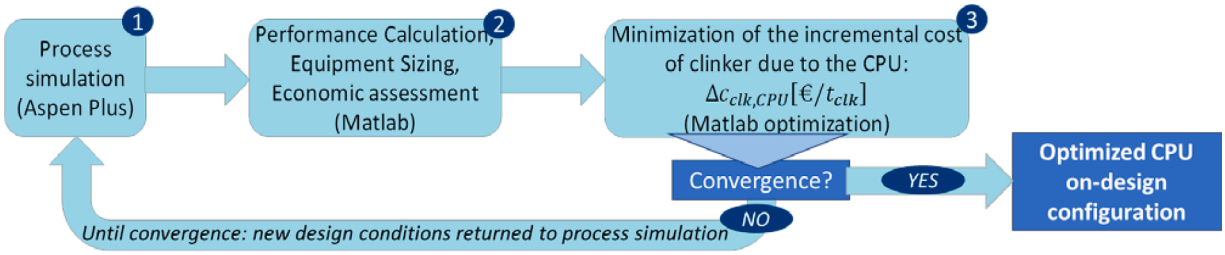


**Fig. 3.** Techno-economic optimization methodology.

- The multi-flow heat exchangers are assumed to be Brazed Aluminum Plate-Fin Heat Exchangers (PFHE), a typical choice for low temperature applications involving $CO_2$ liquefaction or air-related mixtures. This is the reference technology used in the cold boxes of both Callide (Spero et al., 2014) and CIUDEN (Delgado et al., 2014) CPU pilots.

Size and cost of plate-fin heat exchangers are estimated with the B-value method proposed in ESDU 97,006 guidelines (ESDU, 2003). Given the results of the simulation for each stream flowing through the exchanger and assuming the same reference geometry reported in the standard, a mean volumetric heat transfer coefficient $\beta_i$ is evaluated for each stream $i$, by using non-dimensional correlations based on Re and Pr numbers for single-phase streams (reported in ESDU 97,006 guidelines for plate-fin HEX), while evaluating Chen's correlation, based on Martinelli parameter, for two-phase streams (reported in ESDU 97,006 guidelines for plate-fin HEX). The heat exchanger is then split into $z$ zones, and for each of them the zonal average overall volumetric heat transfer coefficient $B_z$ is calculated with Eq. (2):

$$\frac{\dot{Q}_z}{B_z} = \sum_{i=1}^{n} \frac{\dot{Q}_i}{\beta_i} \tag{2}$$

where $\dot{Q}_z$ is the total heat transferred in zone $z$ and $\dot{Q}_i$ is the heat transferred by the $i$-th of the $n$ streams involved in zone $z$. Then, the volume of each zone is obtained from Eq. (3):

$$V_z = \frac{\dot{Q}_z / \Delta T_{m,z}}{B_z} \tag{3}$$

where $\Delta T_{m,z}$ is the zonal logarithmic mean temperature difference. At last, the volume of the heat exchanger is obtained as the sum of the calculated zonal volumes $V_z$, increased by 15% to take into account headers and distributors.

**Table 2**
Summary of the CPU process design and Aspen Plus simulation assumptions.

| Parameter | Value |
|---|---|
| Equation of State | Peng-Robinson |
| Stripping column | Rad-Frac model at the equilibrium |
| Heat losses in multi-flow heat exchangers | 1% |
| Pressure drop in multi-flow heat exchangers | 2% of inlet pressure |
| Minimum process temperature | $T_{CO_2,triple\ point} + 3°C$ |
| Minimum temperature difference in cold box heat exchangers | 1 K |
| Liquid entrainment in the vapor stream separated by flash drums | 1% |
| Intercoolers outlet temperature | 28°C |
| Electricity consumption of cooling system, as a function of rejected heat | 0.01 $kW_{el}/kW_{th}$ |
| Make-up cooling water | 0.61 $kg/MJ_{rejected}$ |
| Dehydration unit recycle rate | 10% |
| Dehydration unit pressure drop | 1 bar |
| Electricity consumption of dehydration unit, as a function of removed water | 2.29 $kWh_{el}/kg_{water}$ |
| Blower outlet pressure | 1.013 bar(a) |
| Blower isentropic efficiency | 0.82 |
| Blower electro-mechanic efficiency | 0.94 |
| Recycle compressor polytropic efficiency | 0.84 |
| Compressor 1.1 polytropic efficiency | 0.87 |
| Compressor 1.2 polytropic efficiency | 0.88 |
| Compressor 1.3 polytropic efficiency | 0.88 |
| Compressor 1.4 polytropic efficiency | 0.86 |
| Compressor 2 polytropic efficiency | 0.85 |
| Recycle compressor polytropic efficiency | 0.84 |
| Compressor 3 polytropic efficiency | 0.84 |
| Compressor 4.1 polytropic efficiency | 0.846 |
| Compressor 4.2 polytropic efficiency | 0.84 |
| Pump polytropic efficiency | 0.84 |
| Compressors and pump electro-mechanic efficiency | 0.95 |
| Stripper pressure drop (gas side) | 0.1 bar |
| Stripping column | Rad-Frac model at the equilibrium |
| Stripper packing | Random packing (pall rings) |

- Pressure drops are estimated according to the ESDU 97,006 guidelines: the cross-section and channel length of each side of the heat exchanger is sized (on-design condition) for a pressure drop of 1% of the inlet pressure for vapor streams, of 0.1 bar for liquid or two-phase streams; in off-design conditions, pressure drops are therefore even lower than the aforementioned values. Then, in process simulations it is conservatively assumed that the overall pressure drop across the heat exchanger is 2% of the inlet pressure (an overestimate of the actual pressure drops occurring both at on-design and off-design conditions), which means that the valves downstream of the heat exchangers (at the outlet of each stream) will regulate their closure to actually match the imposed 2% pressure drop, which remains the same both at on/off-design. For the high purity case study (#201), it is estimated that an additional pressure drop of 1% applied to all the streams of the multi-flow heat exchanger causes an increase of the compression train power by 56 kW, that is a very limited impact on the overall compression consumption (i.e. less than 0.5% of the total power consumed by the CPU).
- The stripper column reboiler is assumed to be a two-stream heat exchanger based on the same PFHE technology.

The diameter of the stripping column is calculated according to criteria by Kister and Gill and by imposing a flooding factor equal to 75%, while the superficial gas velocity at flooding is estimated with the Generalized Pressure Drop Correlation (GPDC) (Kister, 1992). The height of the column is estimated with the Height Equivalent to a Theoretical Plate method (Richardson et al., 2002).

The decision variables changed by the numerical optimizer before step 1 of each new process simulation (see Fig. 3) are reported in Table 3. Each simulation represents a new design for the given CPU scheme, subject to the constraints on thermodynamic feasibility, on the $CO_2$ purity and on the minimum temperature difference in heat exchangers.

### 3.2. Key Performance Indicators and methods for the economic analysis

Three classes of KPIs have been evaluated in this work: energetic, environmental and economic figures of merit.

**Table 3**
Process design variables subject to optimization and their ranges. Quantity refers to Fig. 1 for the moderate purity and Fig. 2 for the high purity scheme.

| Variable for the Moderate purity configuration | Lower bound | Upper bound |
|---|---|---|
| $p_8$: Pressure of stream from the dehydration unit, bar | 20 | 50 |
| $T_{11}$: Inlet temperature to separator 2,°C | −50 | $T_9$ |
| $T_{18} - T_{17}$: Temperature increase of liquid $CO_2$ stream from separator 2 in heat exchanger 2, K | 0 | 30 |
| MITA: Minimum temperature difference in the main heat exchangers, K | 1 | 10 |
| **Variable for the High purity configuration** | **Lower bound** | **Upper bound** |
| $p_8$: Pressure of stream coming from the dehydration unit, bar | 20 | 50 |
| $T_{12}$: Separator inlet temperature,°C | −50 | −35 |
| $p_{15}$: Stripper pressure, bar | 10 | $p_8$ |
| Stripper height (expressed as number of theoretical stages), - | 5 | 15 |
| Split ratio of liquid $CO_2$ into Valves 2 and 3, - | 0.7 | 0.9 |
| $p_{20}$: Valve 2 (low pressure valve) outlet pressure, bar | 6 | $p_{15}$ |
| $T_{14} - T_{13}$: Temperature increase of liquid $CO_2$ stream from the separator in the main heat exchanger, K | 0 | 30 |
| MITA: Minimum temperature difference in the main heat exchanger, K | 1 | 10 |

*CRR* is the $CO_2$ Recovery Ratio (or $CO_2$ Capture Ratio of the CPU), representing the $CO_2$ removal efficiency of the CPU, defined as the ratio between the $CO_2$ recovered by the CPU in the output stream meeting the purity specifications $\dot{m}_{CO_2.rec}$ (stream #CO2-110) and the total $CO_2$ entering the purification unit, $\dot{m}_{CO_2.in}$ (stream #1).

$P_{el,CO_2}$ is the specific electric consumption of the CPU per unit of $CO_2$ recovered, defined as the ratio between the total electric consumption of the CPU $P_{el}[kW_{el}]$ and the recovered $CO_2$ $\dot{m}_{CO_2.rec}\left[\frac{t}{h}\right]$.

$P_{el,clk}$ is the specific electric consumption of the CPU per unit of clinker, defined as the ratio between the total electric consumption of the CPU $P_{el}[kW_{el}]$ and the clinker production rate $\dot{m}_{clk}\left[\frac{t}{h}\right]$.

$CO_2$ purity is defined as the molar fraction of $CO_2$ in the purified stream leaving the CPU.

Different types of $CO_2$ emissions imputable to the CPU are evaluated:

- $e_{CO_2,d}$ are the direct $CO_2$ specific emissions from the CPU, per unit of clinker, defined as the ratio between the $CO_2$ emitted by the CPU (contained in the vent gas) $\left[\frac{kg}{h}\right]$ and the clinker production rate $\dot{m}_{clk}\left[\frac{t}{h}\right]$.
- $e_{CO_2,ind}$ are the indirect $CO_2$ specific emissions due to CPU electricity consumption, per unit of clinker produced.
- $e_{CO_2,eq}$ are the equivalent $CO_2$ specific emissions from the CPU, obtained as the sum of direct and indirect $CO_2$ specific emissions.

The main economic indicator is the incremental cost of clinker reported in eq. (1), which, added to the cost of clinker due to the CAPEX and OPEX of the cement plant and $CO_2$ capture unit (in this case, the CaL system) excluding the CPU ($c_{clk,cem+capture}$), gives the total cost of clinker, $c_{clk}$. In this paper, $c_{clk,cem+capture}$ is calculated according to the assumptions of (De Lena et al., 2019) with fuel costs from (Lindemann Lino, 2020).

The economic assumptions are listed in Table 4, while the equipment and overall plant costing methodology follows the bottom-up approach described in the framework of the CLEANKER project (Lindemann Lino, 2020) and which is typical of preliminary cost assessments. More details on the equipment cost functions, CAPEX and OPEX estimation are reported in the Supplementary material.

Electricity is purchased by the plant at a cost, $c_{el}$, calculated, according to eq. (4), as the sum of a fixed contribution $c_{el,base}$ (assumed equal to the median value for the IG band of Eurostat (Eurostat, 2020), representing the cost at which the heavy industry such as cement manufacturers purchase the electricity in EU) and a variable contribution $c_{el,CO_2}$, which considers carbon tax $c_{CO_2}$ and $CO_2$ intensity $e_{CO_2,el}$.

**Table 4**
Economic assumptions. Details on the methodology for the calculation of the total capital expenditure starting from the evaluation of the equipment cost are reported in the Supplementary material.

| Parameter | Value |
|---|---|
| Capacity factor | 91.3% |
| Tax rate | 0% |
| Operational life | 25 y |
| Construction time | 3 y |
| Percentage of Total Plant Cost depreciated | 100% |
| Inflation rate | 0% |
| Discount rate | 8% |
| Process contingencies – Maturity,% of (*EC* + *IC*) | 20 |
| Process contingencies – Detail Level of equipment list,% of (*EC* + *IC*) | 12 |
| Indirect costs (*INCF*),% of TDC | 14 |
| Owner's costs (*OCF*),% of TDC | 7 |
| Project contingencies ($CF_{project}$),% of TDC | 15 |
| Cost of fuel – Coal | 2.394 €/$GJ_{LHV}$ |
| Cost of fuel – Refuse Derived Fuel | 0.915 €/$GJ_{LHV}$ |
| Cost of fuel – Natural gas | 7.506 €/$GJ_{LHV}$ |
| Cost of electricity, base case ($c_{el,base}$) | 64.84 €/MWh |
| Carbon tax, base case | 50 €/$t_{CO2}$ |
| Carbon intensity of the electric grid | 294.2 $g_{CO2}$/kWh |
| Make-up cooling water cost | 0.39 €/$m^3$ |
| FIXED OPEX: Insurance and local tax | 2% of TPC per year |
| FIXED OPEX: Maintenance cost | 2.5% of TPC per year |

$$c_{el}\left[\frac{€}{MWh}\right] = c_{el,base}\left[\frac{€}{MWh}\right] + \frac{c_{CO_2}\left[\frac{€}{t_{CO_2}}\right]\cdot e_{CO_2,el}\left[\frac{g_{CO_2}}{kWh}\right]}{1000} \quad (4)$$

### 3.3. Case studies description

The two base cases (Moderate and High Purity $CO_2$) have the following basis of design:

- The fuel burnt in the cement plant kiln and in the CaL calciner is pulverized coal (De Lena et al., 2019)
- The target oxygen content at the calciner outlet is 3.5% (dry basis): this value is typical for a cement plant which burns pulverized coal, is equipped with a pre-calciner and where a mechanical transport is used to feed the raw meal;

**Table 5**
Flue gases entering the CPU.

| | Coal(Base case)(De Lena et al., 2019) | Natural gas | RDF | CoalAir infiltrations |
|---|---|---|---|---|
| Gas mass flow rate, kg/s | 37.05 | 32.49 | 40.94 | 39.70 |
| Gas volumetric flow rate, $Nm^3/h$ | 73'903 | 69'082 | 87'358 | 81'293 |
| Dry dust content, g/$Nm^3$ | 47.77 | 54.96 | 40.10 | 43.43 |
| Temperature,°C | 60 | 60 | 60 | 60 |
| Pressure, bar(a) | 0.93 | 0.93 | 0.93 | 0.93 |
| Gas composition,%mol | | | | |
| $CO_2$ | 83.25 | 73.96 | 72.75 | 75.69 |
| $H_2O$ | 11.54 | 21.42 | 21.42 | 10.49 |
| $O_2$ | 3.1 | 2.36 | 3.53 | 4.72 |
| Ar | 1.21 | 1.25 | 1.35 | 1.18 |
| $N_2$ | 0.9 | 1.01 | 0.95 | 7.92 |

- No air infiltrations occur in the calciner line (i.e. calciner, $CO_2$ cooling and recirculation) which operates slightly below the atmospheric pressure, producing $CO_2$-rich flue-gases for the CPU at 0.93 bar (absolute).

The raw $CO_2$ conditions at the CPU inlet are shown in Table 5. The only difference between the two base case assumptions is in the $CO_2$ product quality specifications. The flue gas composition of Table 5 is calculated via process simulations with Aspen Plus for the same reference cement plant as from (De Lena et al., 2019), but with different fuel input and oxygen excess in the combustion region of the calciner. Oxygen excess are: 3.5% for coal, 3% for natural gas, 4.5% for Refuse Derived Fuel.

Sensitivity analyses are carried out to evaluate the impact of the following parameters on the overall techno-economic performance of the CPU:

- **Fuel fed to the oxyfuel calciner**: the options considered in addition to pulverized coal (base case) are natural gas and Refuse Derived Fuel (RDF), the latter representing the most widely used alternative fuel in the cement industry (Global Cement and Concrete Association, 2021). The type of fuel is directly linked to the target oxygen content at the calciner outlet. The flue gases conditions at CPU inlet for different fuel cases are reported in Table 5.
- **Air infiltration rate in the oxyfuel calciner zone**: a dry air intake equal to 10% of the total flue gas flow rate is considered. This case is labelled as 'Coal – Air infiltrations' in Table 5.
- **Minimum temperature difference in cold box heat exchangers**: given the high level of heat integration required in the cold box to achieve optimal techno-economic performance, most of the optimal results are close to the minimum temperature difference allowed in the multi-stream heat exchanger (i.e. 1 K, the minimum value specified by the ESDU technical guidelines). However, in order to explore more practical solutions, of particular interest not only to ensure easier start-up and operability, but also in off-design operation due to air infiltration or change in the flow-rate, a sensitivity is performed by increasing the minimum temperature difference from 1 K to 5 K.
- **Carbon tax**: in addition to the base case value of 50 €/t, a high value of 100 €/t is considered.
- **Carbon intensity of the consumed electricity**: besides the base value of 294.2$g_{CO_2}/kWh$, a halved value, 147.1 $g_{CO_2}$ $/kWh$, representative of a higher RES share in the electricity grid has been considered.

**Table 7**
Optimal design conditions for the base cases optimization.

| | |
|---|---|
| **Optimal values of variables for Base case Moderate Purity (#101)** | |
| $p_8$: Pressure of stream coming from the dehydration unit, bar | 42.0 |
| $T_{11}$: Inlet temperature to separator 2,°C | −49.9 |
| $T_{18} - T_{17}$: Temperature increase of liquid $CO_2$ stream from separator 2 in heat exchanger 2, K | 1.06 |
| MITA: Minimum temperature approach in the main heat exchangers, K | 1.07 |
| **Optimal values of variables for Base case High Purity (#201)** | |
| $p_8$: Pressure of stream coming from the dehydration unit, bar | 28.4 |
| $T_{12}$: Separator inlet temperature,°C | −49.8 |
| $p_{15}$: Stripper pressure, bar | 23.2 |
| Number of theoretical stages in the stripper, - | 14 |
| Split ratio of liquid $CO_2$ into Valves 2 and 3, - | 0.841 |
| $p_{20}$: Valve 2 (low pressure valve) outlet pressure, bar | 6.45 |
| $T_{14} - T_{13}$: Temperature increase of liquid $CO_2$ stream from the separator in the main heat exchanger, K | 25.0 |
| MITA: Minimum temperature approach in the main heat exchanger, K | 1.00 |

The full list of the case studies with their main assumptions is reported in Table 6.

### 3.4. Base case: results and discussion

Table 7 displays the optimal values for the design variables of the moderate and high purity base cases. The energy performance and economic results are summarised in Table 8, while Table 9 reports the

**Table 8**
Optimal KPIs for the base cases optimization.

| | Base case Moderate Purity (#101) | Base case High Purity (#201) |
|---|---|---|
| **Energy-related Key Performance Indicators** | | |
| $CO_2$ Recovery Ratio,% | 99.31 | 96.15 |
| $P_{el}$, MW | 13.51 | 14.66 |
| $P_{el,CO_2}, kWh/t_{CO_2}$ | 112.6 | 126.2 |
| $P_{el,clk}, kWh/t_{clk}$ | 115.1 | 124.9 |
| $CO_2$ purity,%mol | 96.00 | 99.999 |
| **Environmental Key Performance Indicators** | | |
| $e_{CO_2,d}$, $kg_{CO_2}/t_{clk}$ | 7.09 | 39.66 |
| $e_{CO_2,ind}$, $kg_{CO_2}/t_{clk}$ | 33.87 | 36.74 |
| $e_{CO_2,eq}$, $kg_{CO_2}/t_{clk}$ | 40.96 | 76.40 |
| **Economic Key Performance Indicators** | | |
| $\Delta c_{clk,CPU}$, $€/t_{clk}$ | 16.26 | 19.29 |
| $c_{clk}$, $€/t_{clk}$ | 107.48 | 110.51 |

**Table 6**
List of case studies.

| Case ID | Resulting $CO_2$ purity at CPU inlet,%dry | Target purity | Fuel | Air infiltration | Minimum $\Delta T$, K | $CO_2$ tax,€/t $CO_2$ | $CO_2$ intensity of electricity, $kg_{CO_2}/MWh$ |
|---|---|---|---|---|---|---|---|
| Base Moderate Purity − 101 | 94.11 | Moderate | Coal | 0% | > 1 | 50 | 294.2 |
| Base High Purity − 201 | 94.11 | High | Coal | 0% | > 1 | 50 | 294.2 |
| 112 | 94.12 | Moderate | Natural gas | 0% | > 1 | 50 | 294.2 |
| 113 | 92.58 | Moderate | RDF | 0% | > 1 | 50 | 294.2 |
| 212 | 94.12 | High | Natural gas | 0% | > 1 | 50 | 294.2 |
| 213 | 92.58 | High | RDF | 0% | > 1 | 50 | 294.2 |
| 132 | 84.56 | Moderate | Coal | 10% | > 1 | 50 | 294.2 |
| 232 | 84.56 | High | Coal | 10% | > 1 | 50 | 294.2 |
| 143 | 84.56 | Moderate | Coal | 10% | 5 | 50 | 294.2 |
| 243 | 84.56 | High | Coal | 10% | 5 | 50 | 294.2 |
| 153 | 94.11 | Moderate | Coal | 0% | > 1 | 100 | 294.2 |
| 253 | 94.11 | High | Coal | 0% | > 1 | 100 | 294.2 |
| 162 | 94.11 | Moderate | Coal | 0% | > 1 | 100 | 147.1 |
| 262 | 94.11 | High | Coal | 0% | > 1 | 100 | 147.1 |

**Table 9**
Breakdown of $\Delta c_{clk,CPU}$ for Moderate vs High purity base cases (#101 and #201).

| | MP - Base case (#101) | | HP - Base case (#201) | |
|---|---|---|---|---|
| Annualized TPC, €/$t_{clk}$ | 4.57 | 28.1% | 4.98 | 25.8% |
| Water, €/$t_{clk}$ | 0.16 | 1.0% | 0.20 | 1.0% |
| Electricity (carbon tax excluded), € /$t_{clk}$ | 7.45 | 45.8% | 8.08 | 41.9% |
| $CO_2$ tax on indirect emissions from electricity, €/$t_{clk}$ | 1.69 | 10.4% | 1.84 | 9.5% |
| $CO_2$ tax on direct emissions, € /$t_{clk}$ | 0.35 | 2.2% | 1.98 | 10.3% |
| Fixed OPEX, €/$t_{clk}$ | 2.03 | 12.5% | 2.21 | 11.5% |
| **$\Delta c_{clk,CPU}$, €/$t_{clk}$** | **16.26** | | **19.29** | |

breakdown of the incremental clinker cost. The stream tables for the base cases are shown in the Supplementary material. In both cases, the separation temperature is close to −50°C, while the separation pressure is much higher for the lower purity case (therefore characterized by a higher capture efficiency), 42 bar, compared to the 28 bar of the high purity scheme which carries out the distillation at 23 bar. The optimal temperature difference in the cold box HEX is at the minimum bound, i.e. 1 K, suggesting that the thermodynamic optimum is very close to the economic optimum for the CPU, since the energy cost is a significant fraction of the overall construction and operation costs of the CPU. The optimal $CO_2$ recovery rate is extremely high for the moderate purity case (>99%), while the high purity case has the drawback of a higher electricity consumption and lower CRR (96%), which reflects into a higher (+9%) specific energy consumption. As a result, in case the transportation and storage steps impose tighter $CO_2$ purity constraints requiring the installation of a high purity scheme, the incremental cost of clinker increases by 3 €/t, from 16.3 to 19.3 €/$t_{clinker}$. This corresponds to +5–10% of the typical incremental clinker cost due to $CO_2$ capture (according to (De Lena et al., 2019) ranging between 40 and 50 €/$t_{clinker}$ for the CaL technology). As far as the CPU costs are concerned, as highlighted in Table 9 and Fig. 4, the compressor is the key CAPEX item, covering 80% of the Total Plant Cost. However, the additional cost of clinker due to the CPU is mainly driven by the OPEX, with electricity cost (including the $CO_2$ tax on indirect emissions from electricity) being the largest item, accounting between 50% and 55% of the total $\Delta c_{clk,CPU}$ cost. The annualized plant cost weighs between 26 and 28% of the total incremental cost of clinker. High Purity is attained at the expenses of a lower $CO_2$ Recovery Rate which reflects into a higher $CO_2$ tax on direct emissions which covers up to 10% of the $\Delta c_{clk,CPU}$ cost.

### 3.5. Sensitivity analysis on the CPU optimal design: results and discussion

The values of the objective function for all the sensitivity cases are reported in the bar diagrams of Fig. 5 and Fig. 6 and compared against the base case indicators.

The results of the sensitivity analysis on the fuel burned in the calciner are outlined in Table 10 for the Moderate purity cases, while Table 11 summarizes the results for the High Purity cases. The optimal variables do not change significantly when changing the fuel type, while the electricity consumption changes more significantly due to the variation in the raw $CO_2$ mass flow rate to be processed. The CPU electricity consumption for RDF increases compared to coal (from 115 to 122 $kWh/t_{clk}$ for moderate and from 125 to 133 $\frac{kWh}{t_{clk}}$ for high purity), while for natural gas it sharply decreases to 96 $kWh/t_{clk}$ for moderate and to 104 $kWh/t_{clk}$ for the high purity case. This reflects the higher hydrogen to carbon ratio of natural gas compared to coal and the reduced fuel heating value of RDF compared to coal. As a result, the incremental cost of clinker due to CPU is the lowest for natural gas, followed by coal and RDF. However, when the boundary of the analysis is enlarged from the CPU to the entire cement plant with $CO_2$ capture, the fuel cost makes a significant impact and the ranking from the point of view of the overall clinker cost is reversed, with RDF standing out as the least expensive option, 20% less than natural gas.

Table 12 reports the results for the air infiltration cases: 10% air infiltrations to the inlet gases (a value in line with state-of-the-art false air inlet for conventional cement plants) causes a 10 percentage point drop in the $CO_2$ content at the CPU inlet (dry basis) due to the increase in the non-condensable gases content ($O_2$ is 5.3%mol dry, while $N_2$ is 8.8% mol dry). As a result of air infiltrations, the optimal separation pressure for the moderate case is lower (38 bar vs 42 bar) and the minimum temperature higher (close to 1.5 K) compared to the base case. Moreover, the optimal $CO_2$ purity is slightly higher than the bound, i.e. 96.2%, since the constraint on oxygen becomes more stringent than the one on nitrogen. Moving to the high purity case, the key variables with significant changes are the separation pressure, which is raised from 28 to 39 bar, while the stripper pressure is increased by 2 bar up to 25 bar. The $CO_2$ recovery efficiency is significantly affected by air infiltrations and it diminishes with a similar −4.3/4.4% points in both cases, with the moderate case recovering 94.9% of the inlet $CO_2$ and the high purity

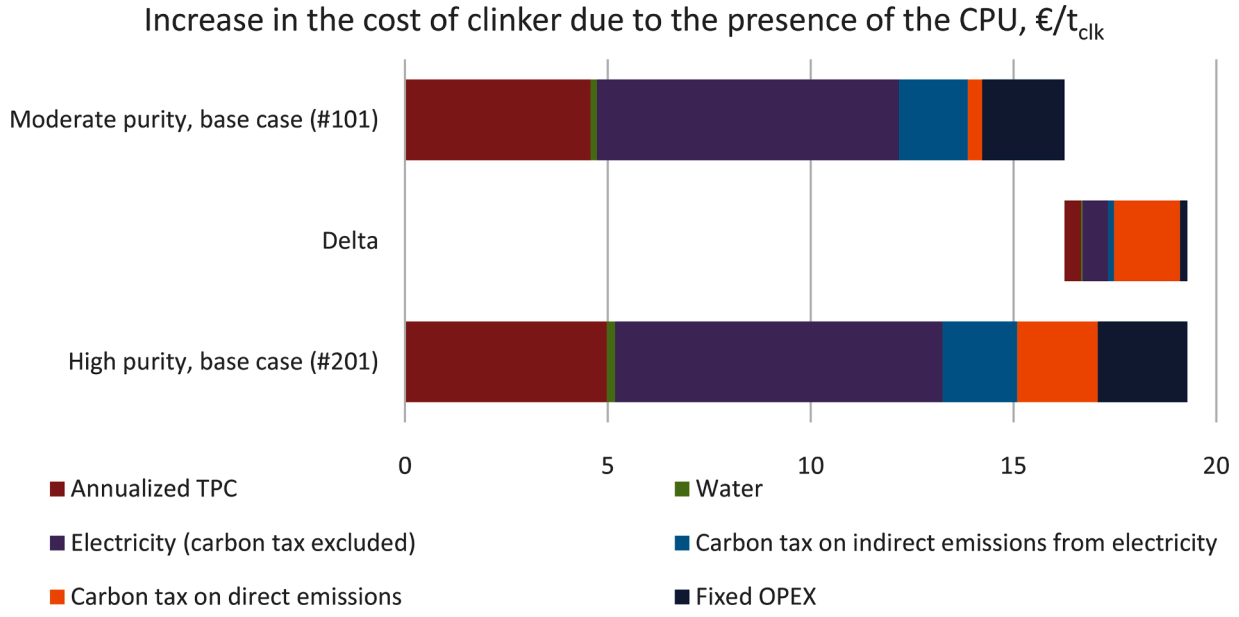


**Fig. 4.** Incremental Cost of clinker, $\Delta c_{clk,CPU}$, breakdown for the optimal CPU Base cases: Moderate (#101) vs High $CO_2$ purity (#201).

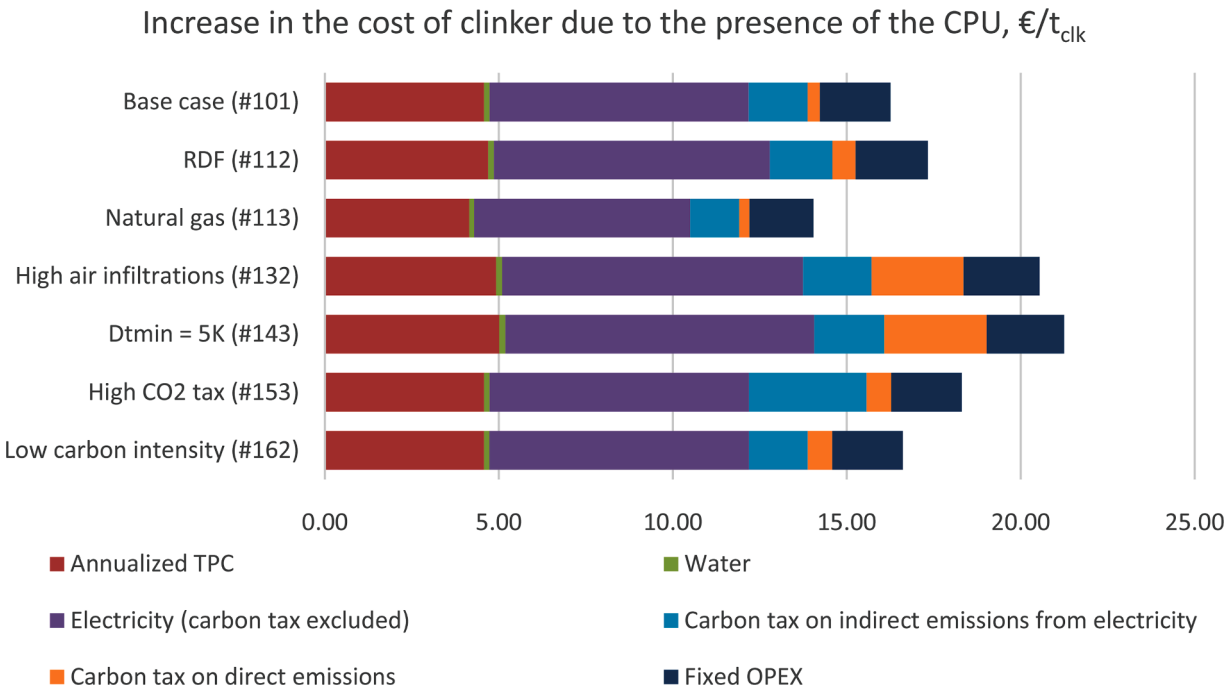


**Fig. 5.** Cases #101, #112, #113, #132, #143, #153, #162 - Moderate purity, sensitivity analysis on fuel, air infiltrations, minimum temperature difference, $CO_2$ tax and carbon intensity. Difference in $\Delta c_{clk,CPU}$.

scheme liquefying only 92.9% of the $CO_2$ captured by the CaL system. In both cases the increase in the cost of clinker is significant, due to the combination of lower recovery rate, higher power consumption and increased capital costs. For the moderate purity case the increase is +26% (from 16.3 to 20.5 $€/t_{clk}$), while for the high purity is +19% (from 19.3 to 23.0 $€/t_{clk}$) featuring a similar absolute increase close to 4 $€/t_{clk}$, which would have a significant impact in terms of clinker decarbonization costs.

The results from the sensitivity on the minimum temperature difference are presented in Table 13 and Fig. 6 making reference to the air infiltration case. When MITA is increased from 1 K to 5 K, in the moderate purity case the CRR reduces from 94.9% to 94.3%, and a similar trend is observed for the high purity case where the $CO_2$ recovery efficiency is slightly reduced from 92.9 to 92.2% and the electricity consumption is marginally increased from 142.7 to 146.3 $kWh/t_{clk}$. As shown in Fig. 6, the clinker cost increases by less than 1 €/t when the design pinch point of the CPU cold box is raised from 1 to 5 K, the main reasons being the slightly higher emissions and hence carbon tax and the

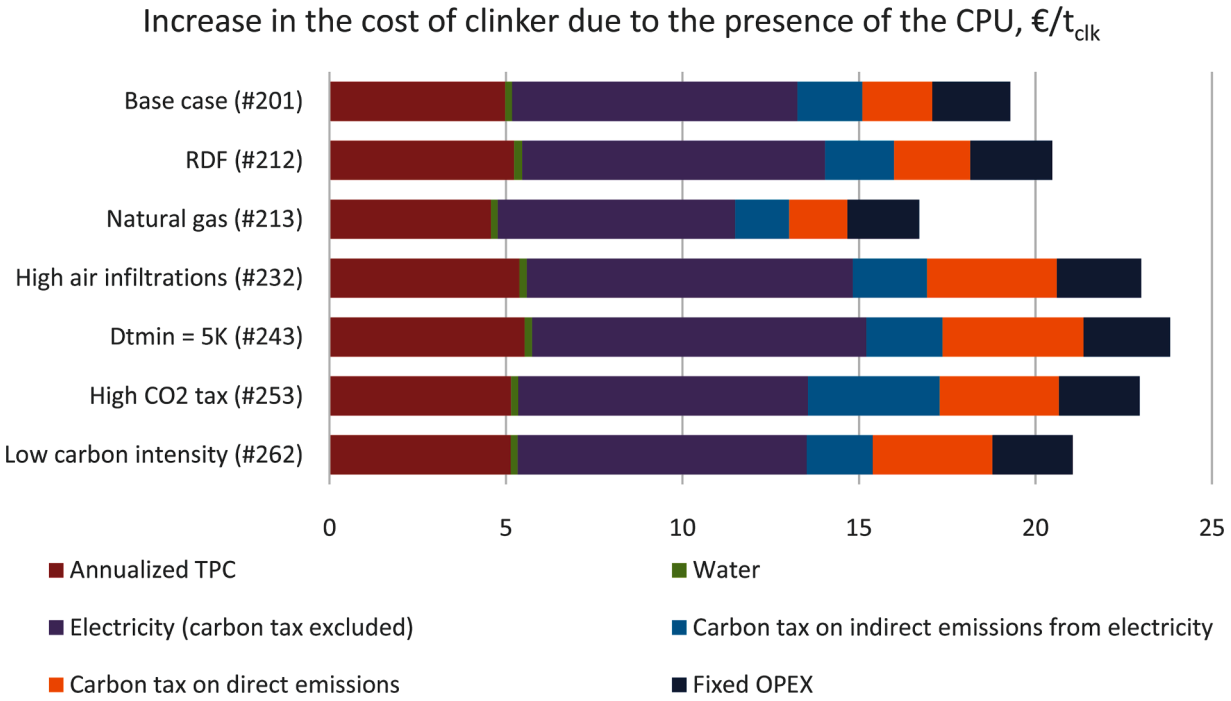


**Fig. 6.** Cases #201, #212, #213, #232, #243, #253, #262 - High purity, sensitivity analysis on fuel, air infiltrations, minimum temperature difference, $CO_2$ tax and carbon intensity. Difference in $\Delta c_{clk,CPU}$.

**Table 10**
Sensitivity analysis on fuel for the Moderate Purity case.

| | Moderate Purity – Base (#101) | Moderate Purity – RDF (#112) | Moderate Purity – Nat. gas (#113) |
|---|---|---|---|
| **Main input data** | | | |
| Fuel | Coal | RDF | Natural gas |
| Gas mass flow rate, kg/s | 37.05 | 40.94 | 32.49 |
| $CO_2$ content in inlet gas,%$mol_{dry}$ | 94.1 | 92.6 | 94.1 |
| $O_2$ content in inlet gas,%$mol_{dry}$ | 3.5 | 4.5 | 3.0 |
| Carbon tax, $€/t_{CO_2}$ | 50 | 50 | 50 |
| $CO_2$ intensity of electricity generation, $kg_{CO_2}/MWh$ | 294.2 | 294.2 | 294.2 |
| **Energy-related Key Performance Indicators** | | | |
| $CO_2$ Recovery Ratio,% | 99.31 | 98.75 | 99.32 |
| $P_{el}$, MW | 13.51 | 14.38 | 11.27 |
| $P_{el,CO_2}$, $kWh/t_{CO_2}$ | 112.6 | 116.7 | 113.1 |
| $P_{el,clk}$, $kWh/t_{clk}$ | 115.1 | 122.5 | 96.0 |
| $CO_2$ purity,%mol | 96.00 | 96.00 | 96.00 |
| **Environmental Key Performance Indicators** | | | |
| $e_{CO_2,d}$, $kg_{CO_2}/t_{clk}$ | 7.09 | 13.24 | 5.81 |
| $e_{CO_2,ind}$, $kg_{CO_2}/t_{clk}$ | 33.87 | 36.05 | 28.25 |
| $e_{CO_2,eq}$, $kg_{CO_2}/t_{clk}$ | 40.96 | 49.30 | 34.06 |
| **Economic Key Performance Indicators** | | | |
| $\Delta c_{clk,CPU}$, $€/t_{clk}$ | 16.26 | 17.33 | 14.05 |
| $c_{clk}$, $€/t_{clk}$ | 107.48 | 102.14 | 127.46 |

**Table 11**
Sensitivity analysis on fuel for the High Purity case.

| | High Purity – Base (#201) | High Purity – RDF (#212) | High Purity – Nat. gas (#213) |
|---|---|---|---|
| **Main input data** | | | |
| Fuel | Coal | RDF | Natural gas |
| Gas mass flow rate, kg/s | 37.05 | 40.94 | 32.49 |
| $CO_2$ content in inlet gas,%$mol_{dry}$ | 94.1 | 82.2 | 83.6 |
| $O_2$ content in inlet gas,%$mol_{dry}$ | 3.5 | 4.5 | 3.0 |
| Carbon tax, $€/t_{CO_2}$ | 50 | 50 | 50 |
| $CO_2$ intensity of electricity generation, $kg_{CO_2}/MWh$ | 294.2 | 294.2 | 294.2 |
| **Energy-related Key Performance Indicators** | | | |
| $CO_2$ Recovery Ratio,% | 96.15 | 95.94 | 96.14 |
| $P_{el}$, MW | 14.66 | 15.56 | 12.21 |
| $P_{el,CO_2}$, $kWh/t_{CO_2}$ | 126.2 | 130.0 | 126.5 |
| $P_{el,clk}$, $kWh/t_{clk}$ | 124.9 | 132.6 | 104.0 |
| $CO_2$ purity,%mol | 99.999 | 99.999 | 99.999 |
| **Environmental Key Performance Indicators** | | | |
| $e_{CO_2,d}$, $kg_{CO_2}/t_{clk}$ | 39.66 | 43.22 | 33.01 |
| $e_{CO_2,ind}$, $kg_{CO_2}/t_{clk}$ | 36.74 | 39.01 | 30.59 |
| $e_{CO_2,eq}$, $kg_{CO_2}/t_{clk}$ | 76.40 | 82.23 | 63.60 |
| **Economic Key Performance Indicators** | | | |
| $\Delta c_{clk,CPU}$, $€/t_{clk}$ | 19.29 | 20.47 | 16.71 |
| $c_{clk}$, $€/t_{clk}$ | 110.51 | 105.28 | 130.12 |

slightly increased electricity consumption. The relatively small increase in the objective function, considering that a 5K minimum temperature difference is a less challenging design parameter for a heat exchanger compared to 1K, suggests that a practical optimal design should not adopt a 1K minimum temperature difference. Less complex and faster start-up and shutdown procedures, as well as an easier CPU operation in general, would probably more than compensate for the slight cost penalty.

The last sensitivity analysis focuses on the impact of the carbon tax and carbon intensity of the electricity mix and it is summarized in Table 14 . Both can be seen as exogenous parameters which do not affect

**Table 12**
Sensitivity analysis on air infiltrations compared to base case. Main input data, optimal values of variables and KPIs.

| | MP – Base (#101) | MP – Air inf. (#132) | HP – Base (#201) | HP – Air inf. (#232) |
|---|---|---|---|---|
| **Main input data** | | | | |
| Fuel | Coal | Coal | Coal | Coal |
| Gas mass flow rate, kg/s | 37.05 | 39.70 | 37.05 | 39.70 |
| $CO_2$ content in inlet gas,%$mol_{dry}$ | 94.1 | 84.6 | 94.1 | 84.6 |
| $O_2$ content in inlet gas,%$mol_{dry}$ | 3.5 | 5.3 | 3.5 | 5.3 |
| Carbon tax, $€/t_{CO_2}$ | 50 | 50 | 50 | 50 |
| $CO_2$ intensity of electricity generation, $kg_{CO_2}/MWh$ | 294.2 | 294.2 | 294.2 | 294.2 |
| **Optimal values of variables** | | | | |
| $p_8$, bar | 42.0 | 37.8 | - | - |
| $T_{11}$,°C | −49.9 | −50.0 | - | - |
| $T_{18} - T_{17}$, K | 1.06 | 3.08 | - | - |
| MITA, K | 1.07 | 1.44 | - | - |
| $p_8$, bar | - | - | 28.4 | 38.6 |
| $T_{12}$,°C | - | - | −49.8 | −50.0 |
| $p_{15}$, bar | - | - | 23.2 | 25.2 |
| Number of stages in the stripper, - | - | - | 14 | 13 |
| Split ratio of liquid $CO_2$ into Valves 2 and 3, - | - | - | 0.841 | 0.825 |
| $p_{20}$, bar | - | - | 6.45 | 6.42 |
| $T_{14} - T_{13}$, K | - | - | 25.0 | 24.6 |
| MITA, K | - | - | 1.00 | 1.01 |
| **Energy-related Key Performance Indicators** | | | | |
| $CO_2$ Recovery Ratio,% | 99.31 | 94.86 | 96.15 | 92.86 |
| $P_{el}$, MW | 13.51 | 15.70 | 14.66 | 16.75 |
| $P_{el,CO_2}$, $kWh/t_{CO_2}$ | 112.6 | 137.0 | 126.2 | 149.3 |
| $P_{el,clk}$, $kWh/t_{clk}$ | 115.1 | 133.7 | 124.9 | 142.7 |
| $CO_2$ purity,%mol | 96.00 | 96.20 | 99.999 | 99.999 |
| **Environmental Key Performance Indicators** | | | | |
| $e_{CO_2,d}$, $kg_{CO_2}/t_{clk}$ | 7.09 | 52.94 | 39.66 | 73.54 |
| $e_{CO_2,ind}$, $kg_{CO_2}/t_{clk}$ | 33.87 | 39.34 | 36.74 | 41.99 |
| $e_{CO_2,eq}$, $kg_{CO_2}/t_{clk}$ | 40.96 | 92.28 | 76.40 | 115.52 |
| **Economic Key Performance Indicators** | | | | |
| $\Delta c_{clk,CPU}$, $€/t_{clk}$ | 16.26 | 20.54 | 19.29 | 22.99 |
| $c_{clk}$, $€/t_{clk}$ | 107.48 | 111.77 | 110.51 | 114.22 |

considerably the design and energy consumption of the CPU, as highlighted by the nearly unchanged CRR and specific energy consumption compared to the base case. However, if the carbon tax is doubled from 50 to 100 €/t of $CO_2$, the cost of clinker increases significantly due to the cost for direct and indirect emissions, by 2 €/t of clinker for moderate purity and up to 5 €/t for the high purity case. On the other hand, if the increase of the carbon tax goes along with a reduction of the grid carbon intensity (as it is expected to happen), then the two effects are nearly compensated and the reduction of the indirect $CO_2$ emissions is counterbalanced by the higher price to be paid for the carbon tax. The outcome is that both factors can be considered external and they would not impact the design of the CPU configurations selected in this work, although in terms of cost of clinker the difference may be significant, therefore putting pressure on the overall capture system in order to target higher capture rates or a partial fuel switch to save emission-related costs.

## 4. Off-design analysis

Air infiltration usually occurs in a cement plant, especially in the cyclones, pre-calciner and pre-heating tower (Zeman, 2009), due to their operation at slight sub-atmospheric pressures and because they are not fully air-tight. Air infiltrations are limited after the ordinary maintenance (typically once a year) and they cause limited efficiency losses in the operation of the cement plant.

By contrast, air infiltrations have an impact on the performance and

**Table 13**
Sensitivity analysis on minimum temperature difference - High purity. Main input data, optimal values of variables and KPIs.

| | Moderate Purity – Air infilt. 1K (#132) | Moderate Purity – Air infilt. 5K (#143) | High Purity – Air infilt. 1K (#232) | High Purity – Air infilt. 5K (#243) |
|---|---|---|---|---|
| **Main input data** | | | | |
| Fuel | Coal | Coal | Coal | Coal |
| Gas mass flow rate, kg/s | 39.70 | 39.70 | 39.70 | 39.70 |
| $CO_2$ content in inlet gas,%$mol_{dry}$ | 84.6 | 84.6 | 85.6 | 85.6 |
| $O_2$ content in inlet gas,%$mol_{dry}$ | 5.3 | 5.3 | 5.3 | 5.3 |
| **Energy-related Key Performance Indicators** | | | | |
| $CO_2$ Recovery Ratio,% | 94.86 | 94.28 | 92.86 | 92.24 |
| $P_{el}$, MW | 15.70 | 16.10 | 16.75 | 17.18 |
| $P_{el,CO_2}$, $kWh/t_{CO_2}$ | 137.0 | 141.3 | 149.3 | 154.1 |
| $P_{el,clk}$, $kWh/t_{clk}$ | 133.7 | 137.1 | 142.7 | 146.3 |
| $CO_2$ purity,% mol | 96.20 | 96.21 | 99.999 | 99.999 |
| **Environmental Key Performance Indicators** | | | | |
| $e_{CO_2,d}$, $kg_{CO_2}/t_{clk}$ | 52.94 | 58.84 | 73.54 | 79.89 |
| $e_{CO_2,ind}$, $kg_{CO_2}/t_{clk}$ | 39.34 | 40.35 | 41.99 | 43.06 |
| $e_{CO_2,eq}$, $kg_{CO_2}/t_{clk}$ | 92.28 | 99.19 | 115.52 | 122.95 |
| **Economic Key Performance Indicators** | | | | |
| $\Delta c_{clk,CPU}$, €/$t_{clk}$ | 20.54 | 21.25 | 22.99 | 23.81 |
| $c_{clk}$, €/$t_{clk}$ | 111.77 | 112.47 | 114.22 | 115.04 |

design of the CPU section when oxyfuel-based $CO_2$ capture is integrated with a cement plant. The full-scale CaL calciner and the related $CO_2$ recirculation line operate slightly sub-atmospheric and they are expected to be exposed to air infiltrations, especially in components such as cyclones and where inspection points are located. Off-design analysis is relevant since the CPU is expected to operate with flow rates coming from the CaL system periodically changing on a yearly basis (i.e. between two maintenance periods) due to air infiltration rates, and growing from a minimum right after maintenance to a maximum right before maintenance.

This section aims at assessing the technical and economic effect of air infiltration on the CPU, which is forced to operate under off-design conditions as a result of the change in flow rate and composition caused by air infiltration.

On and Off-design conditions are defined as follows:

- The CPU design and sizing are optimized for the worst case scenario: condition with the highest inlet flow-rate and the lowest $CO_2$ concentration, representing the situation with the maximum air infiltration (occurring right before maintenance). Optimization is performed for this condition, which is named **"On-design"** and is carried out for the "Coal – Air Infiltrations" cases of Table 5 and Table 6 (#132, #232, #143, #243, which differ each other from the point of view of the scheme and of the minimum temperature difference).
- **"Off-design"** is the situation right after maintenance (i.e. taking place once a year, at time =0, =1 year, =2 years, etc.), when there is no air infiltration and the raw $CO_2$ stream conditions corresponds to the "Base case" of Table 5.
- The composition and flow rate processed by the CPU varies linearly over time (on a yearly basis) assuming that air infiltration changes from 0% (off-design case) to 10% (on-design case) of the flue gas flow-rate leaving the calciner. Therefore, the flow rate processed by the CPU follows the linear sawtooth profile reported in blue in Fig. 7.
- In off-design, the CPU process configuration remains the same as from the on-design optimization, but the process conditions will change according to the new flow rate and composition imposed (see Table 5) and the control strategy adopted for the plant.

Two cases are studied to analyse the off-design behavior of moderate and high purity configurations: the on-design starting conditions are the optimal ones for cases #143 and #243 (see Table 6).

Both designs are based on a MITA of 5 K in the multi-stream HEX. This assumption is taken in order to avoid operability issues resulting from the tighter pinch points obtained in off-design. Indeed, cases with MITA of 1 K have been initially assessed and then excluded because of

**Table 14**
Sensitivity analysis results on carbon tax (CT).

| | Moderate purity - Base (#101) | Moderate purity - High $CO_2$ Tax (#153) | Moderate purity – Low Carbon Intensity (#162) | High Purity - Base (#201) | High purity - High $CO_2$ Tax (#253) | High purity – Low Carbon Intensity (#262) |
|---|---|---|---|---|---|---|
| **Main input data** | | | | | | |
| Fuel | Coal | Coal | Coal | Coal | Coal | Coal |
| Gas mass flow rate, kg/s | 37.05 | 37.05 | 37.05 | 37.05 | 37.05 | 37.05 |
| $CO_2$ content in inlet gas,%$mol_{dry}$ | 94.1 | 94.1 | 94.1 | 94.1 | 94.1 | 94.1 |
| $O_2$ content in inlet gas,%$mol_{dry}$ | 3.5 | 3.5 | 3.5 | 3.5 | 3.5 | 3.5 |
| Carbon tax, €/$t_{CO_2}$ | 50 | 100 | 100 | 50 | 100 | 100 |
| $CO_2$ intensity of electricity generation, $kg_{CO_2}/MWh$ | 294.2 | 294.2 | 147.1 | 294.2 | 294.2 | 147.1 |
| **Energy-related Key Performance Indicators** | | | | | | |
| $CO_2$ Recovery Ratio,% | 99.31 | 99.31 | 99.31 | 96.15 | 96.72 | 96.70 |
| $P_{el}$, MW | 13.51 | 13.51 | 13.52 | 14.66 | 14.89 | 14.86 |
| $P_{el,clk}$, $kWh/t_{clk}$ | 115.1 | 115.1 | 115.2 | 124.9 | 126.8 | 126.6 |
| $CO_2$ purity,%mol | 96.00 | 96.00 | 96.00 | 99.999 | 99.999 | 99.999 |
| **Environmental Key Performance Indicators** | | | | | | |
| $e_{CO_2,d}$, $kg_{CO_2}/t_{clk}$ | 7.09 | 7.08 | 7.07 | 39.66 | 33.80 | 33.94 |
| $e_{CO_2,ind}$, $kg_{CO_2}/t_{clk}$ | 33.87 | 33.87 | 16.95 | 36.74 | 37.32 | 18.62 |
| $e_{CO_2,eq}$, $kg_{CO_2}/t_{clk}$ | 40.96 | 40.95 | 24.01 | 76.40 | 71.12 | 52.56 |
| **Economic Key Performance Indicators** | | | | | | |
| $\Delta c_{clk,CPU}$, €/$t_{clk}$ | 16.26 | 18.31 | 16.61 | 19.29 | 22.95 | 21.06 |
| $c_{clk}$, €/$t_{clk}$ | 107.48 | 110.90 | 108.49 | 110.51 | 115.54 | 112.93 |

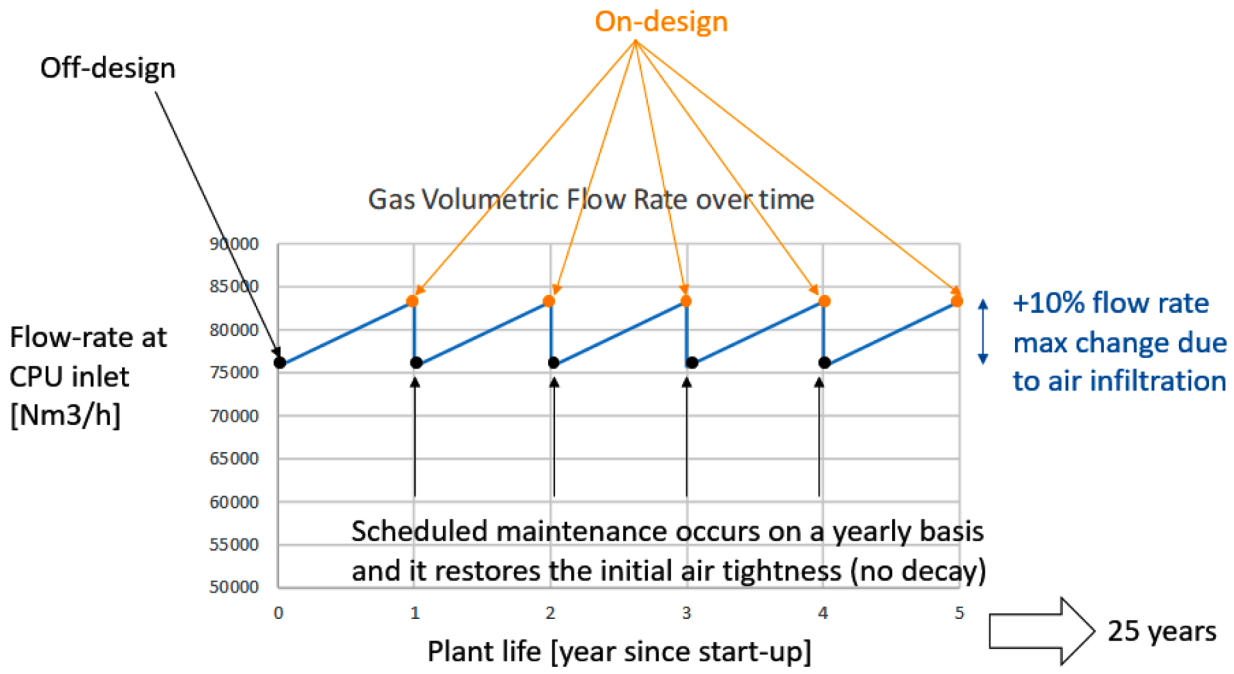


**Fig. 7.** Profile of the gas volumetric flow rate entering the CPU over time: yellow points represent the on-design condition, while black points are the off-design condition assessed right after maintenance. CPU energy consumption, capture rate and other KPIs are assumed to change linearly in between these two points.

pinch points approaching 0 K under off-design conditions.

### 4.1. *Off-design methodology: CPU control strategy*

The off-design conditions and performances are computed according to the following control strategy:

- The main heat exchanger geometry (the term U•A, product between the overall heat transfer coefficient and the heat transfer area) is defined by on-design optimization. Since HEX is a multi-stream compact-type heat exchanger, multiple hot and cold streams exchange heat in parallel. To represent the streams arrangement also in off-design, the on-design multi-stream HEX is replaced by an equivalent network of two-streams heat exchangers, overall transferring the same thermal power of the multi-stream HEX and obtaining the same hot/cold streams final temperatures, with topology and intermediate conditions defined by the "minimum number of units" criterion from Pinch Analysis (i.e. single hot and cold streams are matched based on their thermal capacity and temperature interval, in order to minimize the number of two-stream heat exchanger units required). With this approach, the network replaces the multi-stream HEX while reproducing the same UA, its inlet/outlet temperatures and the overall thermal power exchanged.

  In off-design, the network and geometry are given by the on-design configuration, while the heat exchangers are re-simulated in Aspen Plus with fixed UA, per each subsection, but considering the new streams flow rates, compositions and inlet conditions. The outlet temperature from the heat exchangers and the overall Q transferred will change accordingly. In particular, the adoption of a constant heat transfer coefficient for the PFHE heat exchanger during the off-design analysis is supported by the following considerations: for single-phase streams, ESDU (ESDU, 2003) reports a non-dimensional correlation involving Nu, Re and Pr numbers, in which the exponent of Re, and therefore of the flow-rate, is close to 0.5. As a result, if the flow-rate changes by 10%, the convective heat transfer coefficient shall change by less than 10%; on the other hand, for two-phase streams, ESDU suggests a conservative approach derived from Chen's correlation based on Martinelli parameter, in which a corrected liquid-like heat transfer coefficient is used in place of the two-phase one. As reported in Table 5, the 10% volumetric flow-rate change caused by air infiltration translates into a 7% increase of the mass flow-rate (i.e. from 37.05 to 39.70 kg/s), due to the reduced molecular mass of air compared to the $CO_2$-rich stream to be purified.

- The separator and column stages are assumed to be at the equilibrium under the new conditions (same pressure, but slight change in T and flow-rate profiles).
- For the high purity case, the column reboiler is regulated to keep the $CO_2$ purity in specification (10 ppm $O_2$), with a bypass on the hot side of the HEX which operates at fixed UA.
- Liquid $CO_2$ throttling valves are regulated to get a separation temperature of the two-phase stream close to on-design conditions (i.e. throttling valve pressure is increased in off-design, since the flow-rate is reduced and, consequently the pinch points of HEX are lowered).
- Compressors are regulated as follows:
  - The moderate purity case includes one blower, four intercooled centrifugal compressors (two of them, #1 and #2 in Fig. 2, multi-stage) and one centrifugal pump. Each of these six units is equipped with speed control based on Variable Frequency Drivers.
  - The high purity case includes one blower, five intercooled centrifugal compressors (three of them, #1, #2 and #4 in Fig. 2, multi-stage) and one centrifugal pump. Each of these seven units is equipped with Variable Frequency Drivers.
  - On-design turbomachinery efficiencies are specified in Table 3.
  - The normalized characteristic curves of compressors have been regressed from Atlas Copco chart (see Fig. 8) (Atlas Copco, 2017).
  - In off-design operation, compressors efficiencies and pressure ratios vary according to the "variable speed" control strategy: the compressors operate at volumetric part-load (i.e. lower volumetric flow rate compared to the design point) due to the lower flow-rate, except for the recycle compressor of the high purity case (that have higher volumetric flow rate). The part-load point is at constant pressure ratio for the compressor group (i.e. the operating point

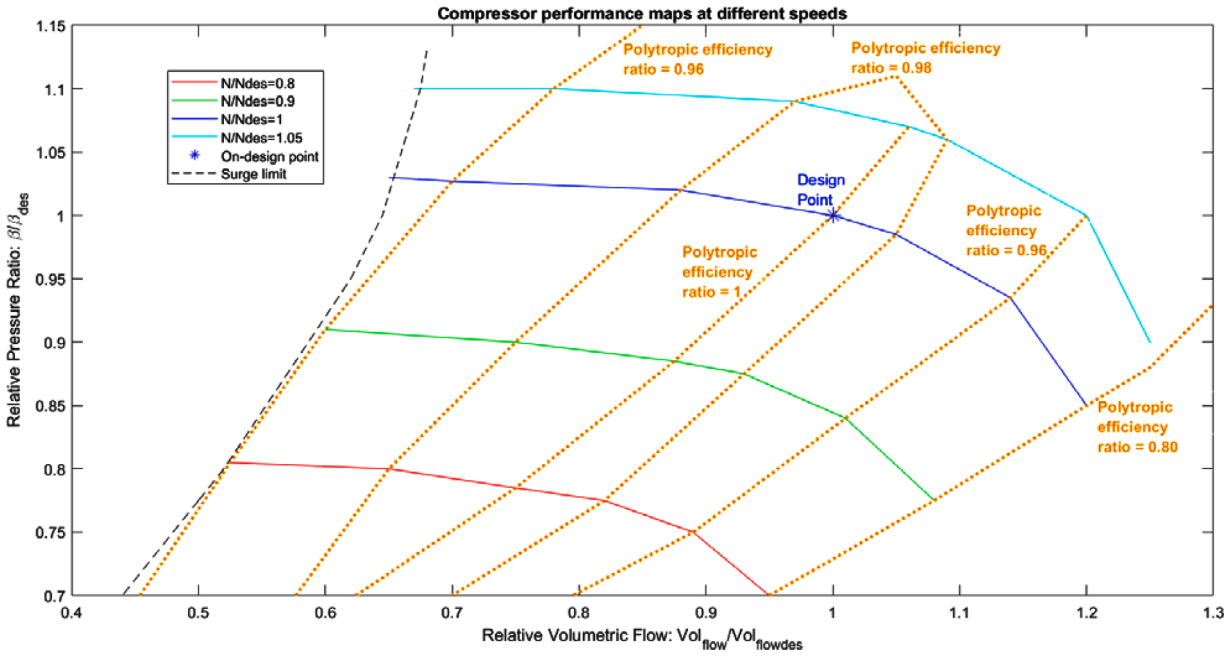


**Fig. 8.** Normalized compressor performance maps regressed from Atlas Copco curves for $CO_2$ compressors. Orange dot curves delimit the regions based on the polytropic efficiency (ratio referred to on-design efficiency). The design point represents the on-design conditions for all the centrifugal compressors considered, while each curve corresponds to a different rotational speed N (Ndes stands for the design speed).

moves horizontally from rated design point to the left in Fig. 8), except for the pump and compressors #3 and #4, which will operate at different compression ratio β, based on the pressure change of the throttling valves. Once the off-design pressure ratios and volumetric flow rate are known, the off-design speed can be calculated, by locating the off-design point of each compressor on the performance chart of Fig. 8. Surge limit shall be always verified.

### 4.2. Off-design results

Table 15 summarizes the key results with air infiltrations. On-design refer to the optimized design conditions of cases #132 and #232 in Table 6. Techno-economic results are shown in Fig. 9.

When moving from off-design to on-design operation, the incremental cost of clinker increases by more than 3 €/t due to the reduced $CO_2$ recovery, since the $CO_2$ stream is more diluted by air infiltration and the overall flow-rate to be compressed increases.

The off-design operational points are reported on the non-dimensional compressor map of Fig. 10 for the high purity case #243. The graph highlights the changes in the compression ratio and volumetric flow-rate for each compressor group compared to the design point.

## 5. Conclusions

This work presents the process design and techno-economic optimization of the $CO_2$ Purification Unit for cement plants equipped with oxy-fuel based calcination. Two alternative schemes are proposed and simulated for the CPU of the integrated CaL process, double-flash autorefrigerated is selected for the less strict transportation and storage requirements (e.g. pipeline transportation/less strict storage option

**Table 15**
Air infiltration cases: optimization results and key operational variables for on-design conditions and rating results for off-design.

| Parameter - Unit | Optimization On-design Moderate purity Air infiltration (#143) | Optimization On-design High purity Air infiltration (#243) | Rating Off-design Moderate purity No air infiltration (#143 after maintenaince) | Rating Off-design Highpurity No air infiltration (#243 after maintenaince) |
|---|---|---|---|---|
| $CO_2$ stream at CPU inlet (to be purified), kg/s | 39.70 | 39.70 | 37.05 | 37.05 |
| $CO_2$ inlet concentration, %mol dry | 84.6 | 84.6 | 94.1 | 94.1 |
| $CO_2$ recovery efficiency, % | 94.28 | 92.24 | 98.47 | 96.68 |
| $CO_2$ purity,%mol | 96.21 | 99.999 | 97.08 | 99.999 |
| p max, bar | 38.0 | 43.4 | 38.0 | 43.4 |
| T separation,°C | −47.5 | −45.9 | −47.0 | −45.9 |
| MITA, K | 5.00 | 5.00 | 2.68 | 2.2 |
| Electric consumption, MWe | 16.10 | 17.18 | 14.47 | 15.95 |
| Specific electric consumption, kWh/ $t_{CO2\ purified}$ | 141.3 | 154.1 | 121.6 | 136.6 |
| Specific electric consumption, kWh/ $t_{clinker}$ | 137.1 | 146.3 | 123.3 | 135.9 |

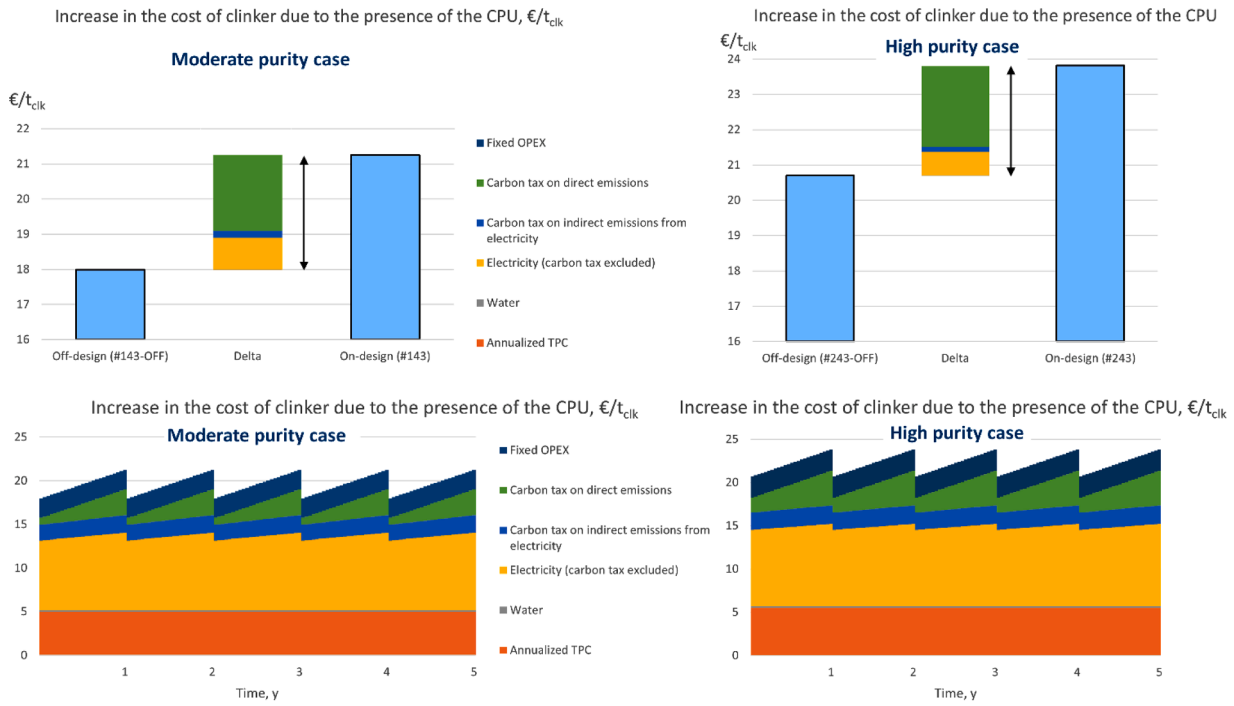


**Fig. 9.** Incremental cost of clinker for the air infiltration cases, highlighting the difference between on and off-design costs (breakdown highlighted in the top bar diagrams). Moderate Purity case (left side) and High purity case (right side) reported. The bottom diagrams highlight the yearly change, and cost-breakdown, of the incremental cost of cleanker between the two maintenance periods, reflecting the flow-rate behavior reported in Fig. 7.

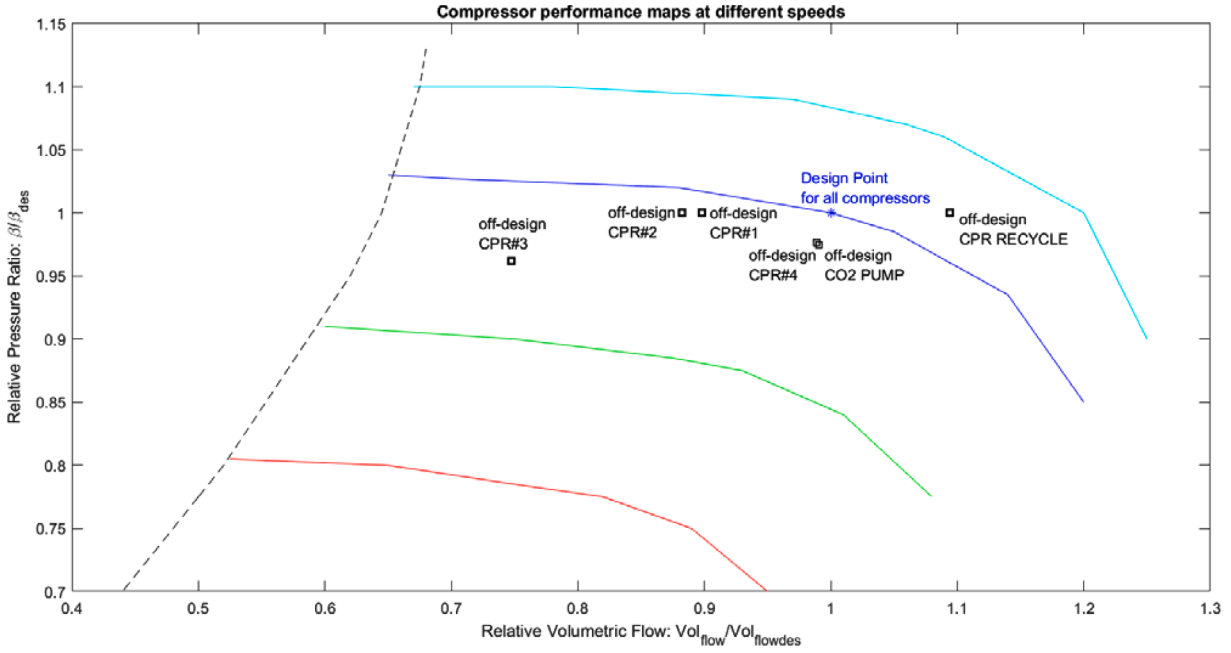


**Fig. 10.** Off-design compressors operational points for the high purity case #243. Black squares show the operating point of each compressor (the blower off-design point is coincident with CPR#1 point).

named "moderate purity"), while distillation-based autorefrigerated is chosen for the more stringent quality specifications (e.g. satisfying the requirements for ship transportation/EOR or high purity $CO_2$ utilisation) option. For both CPU schemes, a base case, focusing on coal-fired cement plant with integrated CaL, is optimized from a technical and economic perspective. Sensitivity cases, highlighting how the optimal design and costs change depending on different scenarios (fuel type, carbon tax and carbon intensity of the electricity consumed), are calculated with the same techno-economic optimization methodology of the base case. Finally, the impact of air infiltration is assessed, not only in terms of design optimization but also by evaluating how the performance and cost of the CPU would change under off-design operation, i.e. when air entrance changes from zero to maximum between two scheduled maintenance periods.

The following main conclusions can be drawn concerning the design of the CPU for a full-scale CaL process, with reference to the base case

input data:

- For a new cement plant equipped with CaL CCS, the economic impact of the CPU on the total clinker cost is not negligible and close to 15%.
- The energy efficiency of the CPU process is the key driver for the techno-economic optimization; the best moderate purity configuration consumes 113 $kWh_{el}/t_{CO2\ purified}$ while the high purity one requires 126 $kWh_{el}/t_{CO2\ purified}$. The recovery rate is very high and reaches >99% if few percentage points of $O_2$ are allowed in the $CO_2$ product, while drops to 96% in the high purity case.
- The optimal separation temperature is the lowest technically achievable, i.e. −50°C, while the separation pressure is typically higher for the two flash-based moderate purity scheme, i.e. close to 40 bar, and lower for the stripper-based high purity scheme, i.e. close to 30 bar. The optimal stripper pressure for high purity is in the range 23–25 bar.
- Although electricity OPEX is the main cost item, covering about half of the incremental cost of clinker, and the CPU capital cost contributes for just one third to $\Delta c_{clk,CPU}$, the largest share of the total CPU CAPEX, nearly 80%, is due to compressors only.

Concerning the air infiltrations cases, the following main results have been obtained:

- Air infiltrations have a major impact on both the incremental cost of clinker due to the CPU (+ 25% when air leakage is increased from 0 to 10%) and the $CO_2$ recovery rate, which is reduced by more than 4% points (for Moderate purity down to nearly 95%, while for High purity to nearly 92%). Thus, the gas-tightness of the oxy-fired zone of the CaL system is crucial to keep $CO_2$ purification costs as low as possible.
- When air infiltrations are expected, to ensure that the CPU can be properly operated and $CO_2$ specifications are met, the CPU design shall be performed for the situation right before maintenance, i.e. oversizing the CPU for all the other operational timeframes and keeping larger pinch point values (e.g. closer to 5 K rather than to 1 K).
- The incremental cost of clinker due to CPU changes by 3 €/$t_{clk}$ when moving from off- to on-design, a significant impact, which may force either to an improved and air-tight design of the calciner or to perform maintenance to remove air-leakages more frequently in case of future increases of the $CO_2$ tax cost or electricity cost.

## Declaration of Competing Interest

The authors declare that they have no known competing financial interests or personal relationships that could have appeared to influence the work reported in this paper.

## Acknowledgements

This project has received funding from the European Union's Horizon 2020 research and innovation programme under grant agreement No 764816. This work is supported by the China Government (National Natural Science Foundation of China) under contract No. 91434124 and No. 51376105.

Disclaimer: The European Commission support for the production of this publication does not constitute endorsement of the contents which reflects the views only of the authors, and the Commission cannot be held responsible for any use which may be made of the information contained therein.

## Supplementary materials

Supplementary material associated with this article can be found, in the online version, at doi:10.1016/j.ijggc.2022.103591.

## References

AMEC, 2015. TVU CCS. WP5 - Onshore Infrastructure. Pipeline network CO2 quality specification.

AspenTech, 2019. Aspen Plus v10. www.aspentech.com (accessed September 2018).

Atlas Copco, 2017. Driving Centrifugal Compressor Technology. http://www.atlascopco-gap.com/fileadmin/user_upload/B_H_2017_Compressor_Brochure.pdf. (Accessed July 2019).

Atsonios, K., Grammelis, P., Antiohos, S.K., Nikolopoulos, N., Kakaras, E., 2015. Integration of calcium looping technology in existing cement plant for CO 2 capture: process modeling and technical considerations. Fuel 153, 210–223. https://doi.org/10.1016/j.fuel.2015.02.084.

Berstad, D., Trædal, S., 2018. Membrane-assisted CO2 liquefaction for CO2 capture from cement plants. Deliverable D11.3 of the HORIZON 2020 project CEMCAP. EC Grant agreement no: 641185.

Besong, M.T., Maroto-Valer, M.M., Finn, A.J., 2013. Study of design parameters affecting the performance of CO2 purification units in oxy-fuel combustion. Int. J. Greenh. Gas Control 12, 441–449. https://doi.org/10.1016/j.ijggc.2012.11.016.

Bliss, K.; Eugene, D.; Harms, R.W.; Carrillo, V.G.; Coddington, K.; Moore, M.; Harju, J.A.; Jensen, M.D.; Botnen, L.S.; Marston, P.; Louis, D.; Melzer, S.; Drechsel, C.; Whitman, L.; Moody, J. A Policy, Legal, and Regulatory Evaluation of the Feasibility of a National Pipeline Infrastructure for the Transport and Storage of Carbon Dioxide; Topical Report for Southern States Energy Board; Interstate Oil and Gas Compact Commission: Oklahoma City, OK, Dec 2010.

Brownsort, D.P.A., 2019. CCUS Projects Network: 1st Report of the Thematic Working Group on: CO2 transport, storage and networks. https://www.ccusnetwork.eu/sites/default/files/TG3_Briefing-CO2-Specifications-for-Transport.pdf. (Accessed June 2020).

Bui, M., Adjiman, C.S., Bardow, A., Anthony, E.J., Boston, A., Brown, S., Fennell, P.S., Fuss, S., Galindo, A., Hackett, L.A., Hallett, J.P., Herzog, H.J., Jackson, G., Kemper, J., Krevor, S., Maitland, G.C., Matuszewski, M., Metcalfe, I.S., Petit, C., Puxty, G., Reimer, J., Reiner, D.M., Rubin, E.S., Scott, S.A., Shah, N., Smit, B., Trusler, J.P.M., Webley, P., Wilcox, J., Mac Dowell, N., 2018. Carbon capture and storage (CCS): the way forward. Energy Environ. Sci. 11, 1062–1176. https://doi.org/10.1039/C7EE02342A.

Burchhard, U., Griebe, S., 2013. Tests and Results of Vattenfall's Oxy-fuel Pilot Plant. In: IEAGHG Oxyfuel Combustion Conference 3 (OCC3), Ponferrada, Spain. 9-13th September 2013.

Carrasco-Maldonado, F., Spörl, R., Fleiger, K., Hoenig, V., Maier, J., Scheffknecht, G., 2016. Oxy-fuel combustion technology for cement production - State of the art research and technology development. Int. J. Greenh. Gas Control. https://doi.org/10.1016/j.ijggc.2015.12.014.

De Lena, E., Magli, F., Spinelli, M., Gatti, M., Lindemann Lino, M., Hoenig, V., Romano, M.C., 2021. Comparative Analysis of the Oxyfuel and Calcium Looping Processes for Low-Carbon Cement Production. In: Proceedings of the 15th Greenhouse Gas Control Technologies Conference 15-18 March 2021. https://doi.org/10.2139/ssrn.3811561.

De Lena, E., Spinelli, M., Gatti, M., Scaccabarozzi, R., Campanari, S., Consonni, S., Cinti, G., Romano, M.C., 2019. Techno-economic analysis of calcium looping processes for low $CO_2$ emission cement plants. Int. J. Greenh. Gas Control 82. https://doi.org/10.1016/j.ijggc.2019.01.005.

De Lena, E., Spinelli, M., Martínez, I., Gatti, M., Scaccabarozzi, R., Cinti, G., Romano, M. C., 2017. Process integration study of tail-end Ca-Looping process for CO2 capture in cement plants. Int. J. Greenh. Gas Control 67, 71–92. https://doi.org/10.1016/j.ijggc.2017.10.005.

Delgado, M.A., Diego, R., Alvarez, I., Ramos, J., Lockwood, F., 2014. CO2 balance in a compression and purification unit (CPU). Energy Procedia 63, 322–331. https://doi.org/10.1016/j.egypro.2014.11.035.

Energy Institute, 2010. Good plant design and operation for onshore carbon capture installations and onshore pipelines.

ESDU, 2003. ESDU 97006 with Amendment A. Selection and costing of heat exchangers. Plate-fin type.

European Cement Research Academy, 2016. ECRA CCS Project: Report on Phase IV.A. Duesseldorf. Technical report TR-ECRA-128/2016. https://ecra-online.org/fileadmin/redaktion/files/pdf/ECRA_Technical_Report_CCS_Phase_IV_A.pdf (accessed June 2020).

Eurostat, 2020. Electricity prices for non-household consumers - bi-annual data (from 2007 onwards). https://appsso.eurostat.ec.europa.eu/nui/show.do?dataset=nrg_pc_205&lang=en (accessed June 2020).

Fortum Oslo Varme AS, 2020. FEED Study Report DG3 (redacted version) - Project CCS Carbon Capture Oslo. Oslo.

Gardarsdottir, S.O., De Lena, E., Romano, M., Roussanaly, S., Voldsund, M., Jos, P., Berstad, D., Fu, C., Anantharaman, R., Sutter, D., Gazzani, M., Mazzotti, M., Cinti, G., 2019a. Comparison of technologies for CO2 capture from cement production - part 2: cost analysis. Energies. https://doi.org/10.3390/en12030542.

Gimenez, M., Paxton, C., Cement, L., Wassard, H., Mogensen, O., Paubel, X., Leclerc, M., Cavagné, P., Perrin, N., 2014. The oxycombustion option. Int. Cem. Rev. 37, 37–43.

Global Cement and Concrete Association, 2021. https://gccassociation.org/ (accessed February 2021).

Hills, T., Leeson, D., Florin, N., Fennell, P., 2016. Carbon capture in the cement industry: technologies, progress, and retrofitting. Environ. Sci. Technol. 50, 368–377. https://doi.org/10.1021/acs.est.5b03508.

IEA (2020), Energy Technology Perspectives 2020, IEA, Paris https://www.iea.org/reports/energy-technology-perspectives-2020 (accessed June 2021).

IEAGHG, 2020. The status and challenges of CO2 shipping infrastructures. Technical Report 2020-10.

IEAGHG, 2013. Deployment of CCS in the Cement Industry, 2013/19, December, 2013. https://ieaghg.org/docs/General_Docs/Reports/2013-19.pdf (accessed June 2020).
IEAGHG, 2013. CO2 pipeline infrastructure, 2013/18, December, 2013. https://ieaghg.org/docs/General_Docs/Reports/2013-18.pdf (accessed June 2020).
IEAGHG, 2011. Rotating Equipment for Carbon Dioxide Capture and Storage.
International Energy Agency, 2013. Technology Roadmap. Carbon capture and storage. https://doi.org/10.1007/SpringerReference_7300.
*IPCC*, 2005. In: Metz, B., Davidson, O., de Coninck, H.C., Loos, M., Meyer, L.A. (Eds.), IPCC Special Report on Carbon Dioxide Capture and Storage. Prepared by Working Group III of the Intergovernmental Panel on Climate Change. Cambridge University Press, Cambridge, United Kingdom and New York, NY, USA, p. 442.
ISO 27913, 2016. Carbon dioxide capture, transportation and geological storage — Pipeline transportation systems.
Jamali, A., Fleiger, K., Ruppert, J., Hoenig, V., Anantharaman, R., 2018. Optimised Opearation of an Oxyfuel Cement Plant (D6.1). CEMCAP project deliverable. https://doi.org/10.5281/zenodo.2597114.
Jin, B., Zhao, H., Zheng, C., 2015. Optimization and control for CO 2 compression and purification unit in oxy-combustion power plants. Energy 83, 416–430. https://doi.org/10.1016/j.energy.2015.02.039.
Kennedy, J., Eberhart, R., 1995. Particle Swarm Optimization 1942–1948.
Kim, S., Ahn, H., Choi, S., Kim, T., 2012. Impurity effects on the oxy-coal combustion power generation system. Int. J. Greenh. Gas Control 11, 262–270. https://doi.org/10.1016/j.ijggc.2012.09.002.
Kister, H.Z., 1992. Distillation Design. McGraw-Hill, New York.
Kolster, C., Mechleri, E., Krevor, S., Mac Dowell, N., 2017. The role of CO 2 purification and transport networks in carbon capture and storage cost reduction. Int. J. Greenh. Gas Control 58, 127–141. https://doi.org/10.1016/j.ijggc.2017.01.014.
Komaki, A., Gotou, T., Uchida, T., Yamada, T., Kiga, T., Spero, C., 2014. Operation experiences of oxyfuel power plant in callide oxyfuel project. Energy Procedia 63, 490–496. https://doi.org/10.1016/j.egypro.2014.11.053.
Kunz, O., Wagner, W., 2012. The GERG-2008 wide-range equation of state for natural gases and other mixtures: an expansion of GERG-2004. J. Chem. Eng. Data 57, 3032–3091. https://doi.org/10.1021/je300655b.
Leung, D.Y.C., Caramanna, G., Maroto-Valer, M.M., 2014. An overview of current status of carbon dioxide capture and storage technologies. Renew. Sustain. Energy Rev. 39, 426–443. https://doi.org/10.1016/j.rser.2014.07.093.
Li, H., Yan, J., 2009. Evaluating cubic equations of state for calculation of vapor – liquid equilibrium of CO2 and CO2-mixtures for CO2 capture and storage processes. Appl. Energy 86, 826–836. https://doi.org/10.1016/j.apenergy.2008.05.018.
Lindemann Lino, M., 2020. Definition of cost functions for equipment cost calculations and economic analysis. Milestone MS11 of the HORIZON 2020 project CLEANKER. EC Grant, 764816 agreement no:
Lockwood, T., 2014. Developments in oxyfuel combustion of coal. London, United Kingdom. ISBN: 978-92-9029-561-7. https://usea.org/sites/default/files/082014_Developments%20in%20oxyfuel%20combustion%20of%20coal_ccc240.pdf (accessed September 2019).
Magli, F., Gatti, M., Spinelli, M., Romano, M.C., 2019. Configuration and preliminary performance of the CPU for two different CO2 target purities (Deliverable D5.10 of the CLEANKER project). 10.5281/zenodo.3530716.
Maroto-Valer, M.M., 2010. Develop. Innovation in Carbon Dioxide (CO2) Capture and Storage Technol. 1.
Mezura-Montes, E., Coello Coello, C.A., 2011. Constraint-handling in nature-inspired numerical optimization: past, present and future. Swarm Evol. Comput. 1, 173–194. https://doi.org/10.1016/j.swevo.2011.10.001.
Nemitallah, M.A., Habib, M.A., Badr, H.M., Said, S.A., Jamal, A., Ben-Mansour, R., Mokheimer, E.M.A., Mezghani, K., 2017. Oxy-fuel combustion technology: current status, applications, and trends. Int. J. Energy Res. 41, 1670–1708. https://doi.org/10.1002/er.3722.
Pedersen, M.E.H., 2010. Good parameters for particle swarm optimization HL1001 1–12.
Pipeline and Hazardous Materials Safety Administration, 2021. Annual report mileage for hazardous liquid or carbon dioxide systems. https://www.phmsa.dot.gov/data-and-statistics/pipeline/annual-report-mileage-hazardous-liquid-or-carbon-dioxide-systems (accessed January 2021).
Porter, R.T.J., Fairweather, M., Kolster, C., Mac Dowell, N., Shah, N., Woolley, R.M., 2017. Cost and performance of some carbon capture technology options for producing different quality CO 2 product streams. Int. J. Greenh. Gas Control 57, 185–195. https://doi.org/10.1016/j.ijggc.2016.11.020.
Richardson, J.F., Harker, J.H., Backhurst, J.R., 2002. Coulson and Richardson's Chemical Eng. 2 https://doi.org/10.2524/jtappij.17.111.
Rolfe, A., Huang, Y., Haaf, M., Pita, A., Rezvani, S., Dave, A., Hewitt, N.J., 2018. Technical and environmental study of calcium carbonate looping versus oxy-fuel options for low CO2 emission cement plants. Int. J. Greenh. Gas Control 75, 85–97. https://doi.org/10.1016/j.ijggc.2018.05.020.
Romano, M.C., 2013. Ultra-high CO2 capture efficiency in CFB oxyfuel power plants by calcium looping process for CO2 recovery from purification units vent gas. Int. J. Greenh. Gas Control 18, 57–67. https://doi.org/10.1016/j.ijggc.2013.07.002.
Scaccabarozzi, R., Gatti, M., Martelli, E., 2016. Thermodynamic analysis and numerical optimization of the NET Power oxy-combustion cycle. Appl. Energy 178, 505–526. https://doi.org/10.1016/j.apenergy.2016.06.060.
Seddighi, S., Clough, P.T., Anthony, E.J., Hughes, R.W., Lu, P., 2018. Scale-up challenges and opportunities for carbon capture by oxy-fuel circulating fluidized beds. Appl. Energy 232, 527–542. https://doi.org/10.1016/j.apenergy.2018.09.167.
Shah, M., Degenstein, N., Zanfir, M., Kumar, R., Bugayong, J., Burgers, K., 2011. Near zero emissions oxy-combustion CO2 purification technology. Energy Procedia 4, 988–995. https://doi.org/10.1016/j.egypro.2011.01.146.
Spero, C., Montagner, F., Chapman, L., Ranie, D., Yamada, T., 2014. Callide Oxyfuel Project – Lessons Learned.
Spero, C., Yamada, T., 2018. Callide Oxyfuel Project Final Results.
Strube, R., Manfrida, G., 2011. International Journal of Greenhouse Gas Control CO2 capture in coal-fired power plants — Impact on plant performance. Int. J. Greenh. Gas Control 5, 710–726. https://doi.org/10.1016/j.ijggc.2011.01.008.
Voldsund, M., Gardarsdottir, S.O., De Lena, E., Pérez-Calvo, J.F., Jamali, A., Berstad, D., Fu, C., Romano, M., Roussanaly, S., Anantharaman, R., Hoppe, H., Sutter, D., Mazzotti, M., Gazzani, M., Cinti, G., Jordal, K., 2019. Comparison of technologies for CO 2 capture from cement production—Part 1: technical evaluation. Energies 12. https://doi.org/10.3390/en12030559.
White, V., Allam, R., Miller, E., 2006. Purification of oxyfuel-derived CO2 for sequestration or EOR. In: Eighth Int. Conf. Greenh. Gas Control Technol. (GHGT-8), Trondheim, Norw, pp. 1–6.
White, V., Allam, R.J., 2008. Purification of carbon dioxide. US 2008/0173584A1.
White, V., Wright, A., Tappe, S., Yan, J., 2013. The air products vattenfall oxyfuel CO2 compression and purification pilot plant at schwarze pumpe. Energy Procedia 37, 1490–1499. https://doi.org/10.1016/j.egypro.2013.06.024.
www.cleanker.eu, 2021. http://www.cleanker.eu/ (accessed November 2021).
Xu, M.-X., Wu, H.-B., Wu, Y.-C., Wang, H.-X., Ouyang, H.-D., Lu, Q., 2021. Design and evaluation of a novel system for the flue gas compression and purification from the oxy-fuel combustion process. Appl. Energy 285, 116388. https://doi.org/10.1016/j.apenergy.2020.116388.
Zeman, F., 2009. Oxygen combustion in cement production. Energy Procedia. https://doi.org/10.1016/j.egypro.2009.01.027.

# References


AMEC, 2015. AMEC Foster Wheeler for Tees Valley Unlimited. WP5 - Onshore Infrastructure. Pipeline network CO2 quality specification. http://www.teessidecollective.co.uk/wp-content/uploads/2015/07/WP5-CO2-Spec-2000-0005-DC00-SPC-0001-R1.pdf (accessed September 2019).

Anantharaman, R., Berstad, D., Cinti, G., De Lena, E., Gatti, M., Gazzani, M., Hoppe, H., Martínez, I., Garcia Moretz-Sohn Monteiro, J., Romano, M., Roussanaly, S., Schols, E., Spinelli, M., Størset, S., Os, P. van, Voldsund, M., 2015. CEMCAP framework for comparative techno- economic analysis of CO2 capture from cement plants. Deliverable D3.2 of the HORIZON 2020 project CEMCAP. EC Grant agreement no: 641185.

Buit, L., Ahmad, M., Mallon, W., Hage, F., Zhang, X., Koenen, M., 2009. WP3.1 Report Standards for CO2. Deliverable D3.1.2 of the CO2Europipe project.

CarbonNet Project, 2016. Development of a CO2 specification for a CCS hub network. WSP | Parsons Brinckerhoff Project No 2269886. The State of Victoria 2016. https://www.globalccsinstitute.com/archive/hub/publications/199363/carbonnet-project-development-co2-specification-ccs-hub-network.pdf (accessed September 2019).

Chauvel, A., Fournier, G., Raimbault, C., 2003. Manual of Process Economic Evaluation. Technip Editions, 2003.

De Visser, E., Hendriks, C., Barrio, M., Mølnvik, M.J., Koeijer, G. De, Liljemark, S., Le, Y., Ce, R.M., Morgan, K., 2008. Dynamis CO2 quality recommendations i, 478–484. https://doi.org/10.1016/j.ijggc.2008.04.006

Energy Institute, 2010. Good plant design and operation for onshore carbon capture installations and onshore pipelines. http://cdn.globalccsinstitute.com/sites/default/files/Good%20plant%20design%20and%20operation%20for%20onshore%20carbon%20capture%20installations%20and%20onshore%20pipelines%20Sept%202010%20WEB%20VERSION%20(2).pdf (accessed September 2019).

ESDU, 2003. ESDU 97006 with Amendment A. Selection and costing of heat exchangers. Plate-fin type. https://www.esdu.com/cgi-bin/ps.pl?sess=unlicensed_1220220223941hdg&t=doc&p=esdu_97006a (accessed June 2020). ISBN: 9781862460089.

Gardarsdottir, S.O., De Lena, E., Romano, M., Roussanaly, S., Voldsund, M., Jos, P., Berstad, D., Fu, C., Anantharaman, R., Sutter, D., Gazzani, M., Mazzotti, M., Cinti, G., 2019. Comparison of Technologies for CO2 Capture from Cement Production - Part 2: Cost Analysis. Energies. https://doi.org/10.3390/en12030542

GPSA, 2004. Engineering Data Book. 12th Edition, GPSA.

IEAGHG, 2011. Rotating Equipment for Carbon Dioxide Capture and Storage. 2011/07. https://ieaghg.org/docs/General_Docs/Reports/2011-07.pdf (accessed March 2019).

INGAA Foundation, 2009. Developing a Pipeline Infrastructure for CO2 Capture and Storage: Issues and Challenges. https://www.ingaa.org/File.aspx?id=8574 (accessed June 2020)

ISO 27913, 2016. Carbon dioxide capture, transportation and geological storage — Pipeline transportation systems.

Kohl, A., Nielsen, R., 1995. Gas purification. 5th edition. Gulf Professional Publishing. ISBN: 9780080507200

Lindemann Lino, M., 2020. Definition of cost functions for equipment cost calculations and economic analysis. Milestone MS11 of the HORIZON 2020 project CLEANKER. EC Grant agreement no: 764816.

Maroto-Valer, M., 2010. Developments and innovation in carbon dioxide (CO2) capture and storage technology. Volume 2: Carbon dioxide (CO2) storage and utilisation. CRC press, Woodhead Publishing Limited.

McCollum, D.L., Ogden, J.M., 2006. Techno-Economic Models for Carbon Dioxide Compression, Transport, and Storage. Correlations for Estimating Carbon Dioxide Density and Viscosity. Institute of Transportation Studies, University of California, Davis, Research Report UCD-ITS-RR-06-14. https://itspubs.ucdavis.edu/publication_detail.php?id=1047 (accessed March 2019).

NETL, Shirley, Pamela, and Myles, Paul. Quality Guidelines for Energy System Studies: CO2 Impurity Design Parameters. United States: N. p., 2019. Web. doi:10.2172/1566771

Ole, B., Ciattaglia, I., Claeys, C., Ekström, C., Feraud, A., Haupt, G., Jentsch, N., Koeijer, G. de, Kvamsdal, H., Laffont, P., Papapavlou, C., Panesar, R., Schwendig, F., 2008. Reference cases and guidelines for technology concepts. Deliverable 1.1.1-2 of the ENCAP project.

Oosterkamp, A., Ramsen, J., 2008. State-of-the-Art Overview of CO2 Pipeline Transport with relevance to offshore pipelines.

Santos, S., 2012. CO2 Transport via Pipeline and Ship. https://ieaghg.org/docs/General_Docs/IEAGHG_Presentations/3._CO2_Transport_Overview_-_S._Santos_IEAGHG.pdf (accessed March 2019).

Vermeulen, T.N., 2011. Knowledge Sharing Report 4 - CO2 Liquid Logistics Shipping Concept (LLSC). Overall Supply Chain Optimization. The Rotterdam CCS Network. https://www.globalccsinstitute.com/archive/hub/publications/19011/co2-liquid-logistics-shipping-concept-llsc-overall-supply-chain-optimization.pdf (accessed September 2019).

# Supplementary material

Table A - 1. Review and comparison of the $CO_2$ quality specifications from different sources, projects and CCUS transport and storage modes.

| Source | Transport | | Storage | | $CO_2$ | $H_2O$ | $N_2$ | $O_2$ | Ar | CO | Total inerts | $H_2S$ | $SO_2$ | NOx | Particulates |
|---|---|---|---|---|---|---|---|---|---|---|---|---|---|---|---|
| | Pipeline | Ship | EOR | Geological | vol% (min) | ppmv | vol% | ppmv | vol% | ppmv | vol% | ppmv | ppmv | ppmv | ppmv |
| Weyburn pipeline, EOR (De Visser et al., 2008) | X | | X | | 96 | 20 | 0.03 | 50 | | 1000 | | 9000 | | | |
| Kinder Morgan trade specification, pipeline + EOR (De Visser et al., 2008) | X | | X | | 95.5 | 500 | 4 | 100-1000 | 4 | 2000 | 4 | 200 | 100 | 100 | |
| Sleipner pipeline specification, for offshore sandstone reservoir (De Visser et al., 2008) | X | | | X | 93-96 | Saturated | | | | 3-5 | 150 | | | | |
| DYNAMIS $CO_2$ quality recommendation, pipeline + storage in aquifer (De Visser et al., 2008) | X | | | X | 95.5 | 500 | 4 | 40000 | 4 | 2000 | 4 | 200 | 100 | 100 | |
| ENCAP scenario: pipeline transport and EOR with conservative water content requirement (Ole et al., 2008) | X | | X | | 90 | 50 | 4 | 100 | 4 | 40000 | | 50 | 50 | - | - |
| ENCAP scenario: ship transport and EOR combined with strict limit values for toxics (Ole et al., 2008) | | X | X | | 95 | 5 | 4 | 100 | 4 | 5 | | 5 | 5 | 5 | - |
| ENCAP scenario: pipeline transport and geologic storage (Ole et al., 2008) | X | | | X | 90 | 500 | 4 | 40000 | 4 | 40000 | | 15000 | - | - | - |
| Canyon Reef Carriers pipeline (Oosterkamp and Ramsen, 2008) | X | | | | 85-98 | 50 $ppm_{wt}$ | 0.5 | | | | | 200 | | | |
| Central Basin pipeline (Oosterkamp and Ramsen, 2008) | X | | | | 98.5 | 257 $ppm_{wt}$ | 1.3 | 10 $ppm_{wt}$ | | | 20 | | | | |
| Sheep Mountain pipeline (Oosterkamp and Ramsen, 2008) | X | | | | 96.8-97.4 | 129 $ppm_{wt}$ | 0.6-0.9 | | | | | | | | |
| Cortez pipeline (Oosterkamp and Ramsen, 2008) | X | | | | 95 | | 4 | | | | | 20 | | | |
| US $CO_2$ Pipeline Specifications for EOR (INGAA Foundation, 2009) | X | | X | | 95 | 640 | 4 | 10 | | | | 10-200 | | | |
| $CO_2$EUROPIPE recommendation for pipeline transport (Buit et al., 2009) | X | | | | 95 | No free water | | | 4750 | 5 | 235 | 75 | 75 | | |
| $CO_2$ quality recommendation, pipeline transport + EOR (Maroto-Valer, 2010) | X | | X | | 95.5 | 500 | | | | 2000 | 4 | 200 | | | |
| $CO_2$ quality recommendation, pipeline transport + aquifer storage (Maroto-Valer, 2010) | X | | | X | 95.5 | 500 | | | | 2000 | 4 | 200 | | | |

| | | | | | | | | | | | | | | | |
|---|---|---|---|---|---|---|---|---|---|---|---|---|---|---|---|
| Canyon Reef project advise (Energy Institute, 2010) | X | | | | 95 | 250 $ppm_{wt}$ | 4 | 10 $ppm_{wt}$ | | | 1500 $ppm_{wt}$ | | | | |
| $CO_2$ quality recommendation, ship transport (Maroto-Valer, 2010) | | X | | | 99.7 | 50 | 0.3 | | 0.3 | 2000 | 0.3 | 200 | | | |
| The Rotterdam CCS Network project, recommendations for EOR (Vermeulen, 2011) | | | X | | | | 0.03 | 50 | | | | | | | |
| The Rotterdam CCS Network project, recommendations for low pressure pipeline (Vermeulen, 2011) | X | | | | | 150 | | | | 2000 | 4 | 200 | 100 | 100 | |
| The Rotterdam CCS Network project, recommendations for high pressure pipeline (Vermeulen, 2011) | X | | | | | 500 | | | | 2000 | 4 | 200 | 100 | 100 | |
| The Rotterdam CCS Network project, recommendations for geological storage in gas field (Vermeulen, 2011) | | | | X | | 10 | | 10 | | | | | | | |
| The Rotterdam CCS Network project, recommendations for liquefaction (Vermeulen, 2011) | | X | | | | 10 | | | | | influence the saturation line of CO2 | | | | |
| Dixon Consulting, pipeline + EOR (Santos, 2012) | X | | X | | | -5°C DP @300 psia | 2 | 2 ppmwt | | | | 100 ppmwt | 5 ppmwt | | |
| Industry Working Group, preliminary specifications for pipeline (Santos, 2012) | X | | | | 95 | -40°C DP | 4 | 100 | | 1000 | | 10-200 | | | |
| Dakota Gasification, pipeline (Santos, 2012) | X | | | | 96.8 | 28 lb/MMCF | 4 | 10 | | | | 1500 | | | |
| Strawman Composite, pipeline (Santos, 2012) | X | | | | 97 | 1 | | 2 | | 5000 | | | 5 | | |
| NETL recommendation, EOR (NETL, 2013) | | | X | | 95 | 500 | 1 | 10 | 1 | 35 | | 100 | 100 | 100 | 1 |
| NETL recommendation, carbon Steel Pipeline (NETL, 2013) | X | | | | 95 | 500 | 4 | 10 | 4 | 35 | | 100 | 100 | 100 | 1 |
| NETL recommendation, saline Reservoir Sequestration (NETL, 2013) | | | | X | 95 | 500 | 4 | 10 | 4 | 35 | | 100 | 100 | 100 | 1 |
| NETL recommendation, saline Reservoir CO2 & H2S Co-sequestration (NETL, 2013) | | | | X | 95 | 500 | 4 | 10 | 4 | 35 | | 75 | 50 | 100 | 1 |
| Teesside project recommendation, pipeline, liquid CO2 (AMEC, 2015) | X | | | | 96 | 50 | | 10 | | 2000 | 4 | 20 | 100 | 100 | |
| Teesside project recommendation, pipeline, gaseous CO2 (AMEC, 2015) | X | | | | 91 | 50 | | 10 | | 2000 | 9 | 80 | 100 | 100 | |

| | | | | | | | | | | | | | | | |
|---|---|---|---|---|---|---|---|---|---|---|---|---|---|---|---|
| Teesside project recommendation, pipeline + EOR/Storage (AMEC, 2015) | X | | X | X | 95 | 50 | 1 | 10 | 1 | 2000 | 4 | 200 | 100 | 100 | 1 mg/N m3, < 10 µm |
| CEMCAP assumptions for pipeline (Anantharaman et al., 2015) | X | | | | 95 | | 4 | 40000 | 4 | 35 | | | 100 | 100 | |
| Shell Goldeneye project, pipeline (AMEC, 2015) | X | | | | 99.97 | 50 | 0.0322 | 1 | 0 | 0 | | | 0 | 0 | |
| AMEC project CNS, pipeline (AMEC, 2015) | X | | | | 99 | 40 | | 1 | | 10 | 1 | 20 | 10 | 10 | < 7 µm |
| EON Kingsnorth, pipeline (AMEC, 2015) | X | | | | | 24 | | | | | | | | | |
| NGC Longannet, pipeline (AMEC, 2015) | X | | | | 99 | 50 | 0.6 | 1 | 0.6 | 10 | 1 | 0.5 | 10 | 10 | < 7 µm |
| AMEC project Middle East, pipeline (AMEC, 2015) | X | | | | 99 | 0.3375 g/Nm3 | 0.5 | | | 1800 | | 400 | | | |
| CEMCAP assumptions for ship transport (Anantharaman et al., 2015) | | X | | | 95 | 50 | 4 | 40000 | 4 | 35 | | | 100 | 100 | |
| CarbonNet project proposed specifications, pipeline + geological storage (CarbonNet Project, 2016) | X | | | X | 93.5 | 100 | | | | 900-5000 | 2-5 | 100 | 200-2000 | 250-2500 | |
| ISO 27913:2016, Pipeline transportation systems (ISO 27913, 2016) | X | | | | 95 | 20-630 | 2 | | | 2000 | 4 | 200 | 50 | 50 | |

## CAPEX estimation

The Total plant cost ($TPC$) of each item is estimated by increasing the total direct costs ($TDC$) by the indirect cost factor ($INCF$), the owner's cost factor ($OCF$) and the project contingencies factor ($CF_{project}$). In turn, total direct costs are estimated as the sum of equipment cost ($EC$) and installation cost ($IC$), increased by a process contingency factor ($CF_{process}$) considering both the maturity of the considered techology and the level of detail of the equipment list assumed for the estimation. The equipment cost are estimated by means of the cost functions reported in the next section.

$$TPC = TDC \cdot (1 + INCF + OCF + CF_{project})$$
$$TDC = (EC + IC) \cdot (1 + CF_{process})$$

## Equipment cost functions

The cost function of the baghouse filter has been assumed from (Lindemann Lino, 2020). It provides an estimation of the EPC of the component, including the filter, the fan, conveyors and other minor equipment in a turn-key project. The adoption of non-conventional materials to improve the resistance of the filter housing against corrosion attack is not considered necessary.

$$EPC[€_{2018}] = 1'750 \cdot \dot{V}_{gas\ inlet}^{0.6} \left[\frac{Am^3}{h}\right]$$

Where $\dot{V}_{gas\ inlet}$ is the actual gas volume flow at the bag house inlet, in $Am^3/h$ (where Am$^3$ stands for Actual cubic m).

The cost function of the baghouse filter has been assumed from (Lindemann Lino, 2020), considering sealed machines.

The cost function for the compressor has been derived from (McCollum and Ogden, 2006), and it provides the total plant cost (i.e. installation, process contingencies, indirect costs, owner's costs and project contingencies included).

$$TPC[k€_{2018}] = \dot{m}_{cpr}\left[\frac{kg}{s}\right] \cdot \left[141.9 \cdot \left(\dot{m}_{cpr}\left[\frac{kg}{s}\right]\right)^{-0.71} + 1528.3 \cdot \left(\dot{m}_{cpr}\left[\frac{kg}{s}\right]\right)^{-0.6} \cdot \ln\left(\frac{p_{out}}{p_{in}}\right)\right]$$

Considering the same installation factor as the $CO_2$ pump reported below, as well as the assumptions common to all equipment units, the adopted cost function results in specific equipment costs coherent with the range reported by IEAGHG (IEAGHG, 2011) for in-line $CO_2$ compressors in the 1-10 MW range.

The last compression stage to reach the transport pressure (110 bar) is considered a pump. The cost function reported in (Lindemann Lino, 2020) has been adopted.

$$EC[k€_{2018}] = 1'710 \cdot \left(\frac{P_{design}[kW]}{1'200}\right)^{0.85}$$

$$IC = \frac{2}{3} \cdot EC$$

The stripper column price is a function of the weight and material used. The column is sized as a pressurized stainless steel vessel for which the purchased equipment cost is estimated based on the methodology by Chauvel (Chauvel et al., 2003):

- The vessel thickness, *e*, is calculated with the basic formula:

$$e = e_b + corr_{all} = \frac{p \cdot D/2}{\frac{\sigma}{f} - 0.6p} + corr_{all}$$

, where $corr_{all}$ is the extra thickness for corrosion allowance (equal to 3 mm) and $e_b$ is the base thickness, p is the design pressure of the vessel (operating pressure plus additional pressure due to column completely filled with water, everything increased by a 20% safety factor), D is the column internal diameter, $\sigma$ is the maximum allowable stress of the material (200 MPa) and *f* is the safety factor assumed equal to 2

- The column shell volume and weight are then calculated assuming cylindrical shape and a metal density of 7910 kg/m$^3$
- The vessel cost follows the equation by Chauvel, escalated to year 2018

$$EC_{vessel}[k€_{2018}] = \frac{CEPCI_{2018}}{CEPCI_{2000}} \cdot column\ shell\ weight[kg] \cdot 7.5 \cdot \left(\frac{D}{3}\right)^{-0.21}$$

- The equipment cost of the stripper column is computed by adding to the vessel cost, the cost for packing, accessories and other column internals:
  $EC_{stripper} = EC_{vessel} + EC_{packing} + EC_{access} + EC_{oth\ internals}$,
  , where
  $EC_{packing}[k€_{2018}] = \frac{CEPCI_{2018}}{CEPCI_{2000}} \cdot 65 \cdot \left(\frac{Vol_{packing}}{20}\right)^{0.9}$,
  $EC_{access}[k€_{2018}] = \frac{CEPCI_{2018}}{CEPCI_{2000}} \cdot 22 \cdot \left(\frac{column\ shell\ weight[kg]}{10000}\right)^{0.5}$,
  $EC_{oth\ internals}[k€_{2018}] = 0.15 \cdot \left( EC_{vessel} + EC_{packing} + EC_{access}\right)$

The installation factor has been provided by a technology provider of low-temperature

$CO_2$ strippers

$$IC = EC$$

Since a cooling tower has to be built anyway in order to reject heat from the condenser of the steam cycle, the cost considered here is its increased cost to handle the additional cooling water flow $\dot{m}_{w,CPU}$ needed by the CPU. Equipment cost function and installation factor are derived from (Gardarsdottir et al., 2019). The base cooling water flow $\dot{m}_{w,ref}$ is 1'415.9 l/s, as calculated for the reference plant.

$$EC[k€_{2018}] = 615.56 \cdot \left[\left(\frac{\dot{m}_{w,CPU}\left[\frac{l}{s}\right] + \dot{m}_{w,ref}\left[\frac{l}{s}\right]}{1'239.5}\right)^{0.8} - \left(\frac{\dot{m}_{w,CPU}[l/s]}{1'239.5}\right)^{0.8}\right]$$

$$IC = 0.78 \cdot EC$$

The dehydration unit is based on the molecular sieve technology, and its cost is a function of the molecular sieve containers cost and the estimated adsorbent mass (Lindemann Lino, 2020).

The equipment cost of containers is estimated with the cost function reported below, adapted from (Kohl and Nielsen, 1995), while the amount of sorbent needed is calculated following the simplified approach presented in (GPSA, 2004), assuming 1/8 in. sorbent particles of the bead type.

$$EC_{containers}[k€_{2018}] = 40.7 \cdot \left( \frac{V_{in}\left[\frac{Nm^3}{h}\right]}{1'115.9} \right)^{0.514}$$

$$IC = EC$$

The cost of the 2-streams Plate-Fin Heat Exchanger used as reboiler is assessed by means of the C-method described in (Lindemann Lino, 2020). In case of pressures above 40 bar, the cost is calculated from 25-40 bar data and increased proportionally to the pressure factors presented in (ESDU, 2003).

$$IC = 0.5 \cdot EC$$

Multi-flow heat exchangers are sized following the B-method described in section 3, and the cost is evaluated with the cost function provided by ESDU 97006 (ESDU, 2003). The same installation factor reported by (Lindemann Lino, 2020) for 2-streams PFHEs is assumed.

$$IC = 0.5 \cdot EC$$

The separators are assumed to be stainless steel vessels, and the cost is estimated with the following function, regressed from APEA cost data.

$$EC[k€_{2018}] = 1.95 \cdot sp^{0.6148}$$

Where the sizing parameter $sp$ is closely related to the amount of steel needed, and it is defined as

$$sp = \pi \cdot p[bar] \cdot H[m] \cdot D[m]$$

Where $p$, $H$ and $D$ are the operating pressure, height and diameter of the separator, respectively.

$$IC = EC$$

Table A - 2. Conditions of the main streams for Base Case #101 – Moderate purity, Coal, base case.

| | 1 | 4 | 7 | 8 | 9 | 10 | 11 | 12 | 14 | 16 |
|---|---|---|---|---|---|---|---|---|---|---|
| Temperature, °C | 60.00 | 30.27 | 28.00 | 27.46 | -14.20 | -14.20 | -49.93 | -49.93 | 10.00 | -19.20 |
| Pressure, bar(a) | 0.93 | 20.31 | 42.98 | 41.98 | 41.14 | 41.14 | 40.31 | 40.31 | 38.72 | 39.51 |
| Mass Vapor Fraction, - | 1.000 | 1.000 | 1.000 | 1.000 | 0.062 | 0.869 | 0.299 | 0.977 | 1.000 | 1.000 |
| Mass Density, kg/m$^3$ | 1.4 | 38.9 | 97.8 | 95.1 | 634.3 | 114.8 | 258.3 | 94.3 | 63.2 | 74.7 |
| Mass Flow, kg/s | 37.046 | 35.175 | 39.078 | 35.142 | 35.142 | 2.509 | 2.509 | 0.768 | 0.768 | 0.768 |
| Mole Flow, kmol/s | 0.916 | 0.812 | 0.902 | 0.810 | 0.810 | 0.062 | 0.062 | 0.021 | 0.021 | 0.021 |
| Mole Fractions (wet basis) | | | | | | | | | | |
| $CO_2$ | 0.83254 | 0.93901 | 0.9393 | 0.9411 | 0.9411 | 0.69347 | 0.69347 | 0.24502 | 0.24502 | 0.24502 |
| $H_2O$ | 0.11536 | 0.00223 | 0.00192 | 1E-06 | 1E-06 | 1.8E-07 | 1.8E-07 | 6.7E-09 | 6.7E-09 | 6.7E-09 |
| $N_2$ | 0.00902 | 0.01017 | 0.01018 | 0.0102 | 0.0102 | 0.05753 | 0.05753 | 0.14532 | 0.14532 | 0.14532 |
| $O_2$ | 0.03096 | 0.03492 | 0.03493 | 0.035 | 0.035 | 0.17366 | 0.17366 | 0.42014 | 0.42014 | 0.42014 |
| Ar | 0.01212 | 0.01367 | 0.01367 | 0.0137 | 0.0137 | 0.07535 | 0.07535 | 0.18952 | 0.18952 | 0.18952 |

| | 17 | 18 | 19 | 20 | 21 | 22 | 23 | 24 | 26 | CO2-110 |
|---|---|---|---|---|---|---|---|---|---|---|
| Temperature, °C | -49.93 | -48.87 | -53.17 | -27.05 | 10.00 | -14.20 | -15.52 | 24.57 | 28.00 | 28.00 |
| Pressure, bar(a) | 40.31 | 39.51 | 17.54 | 17.19 | 16.84 | 41.14 | 37.58 | 36.83 | 36.83 | 110.00 |
| Mass Vapor Fraction, - | 0.000 | 0.003 | 0.064 | 0.801 | 1.000 | 0.000 | 0.019 | 1.000 | 1.000 | 1.000 |
| Mass Density, kg/m$^3$ | 1110.4 | 1076.5 | 412.7 | 53.7 | 34.6 | 972.9 | 832.9 | 82.8 | 79.3 | 705.7 |
| Mass Flow, kg/s | 1.741 | 1.741 | 1.741 | 1.741 | 1.741 | 32.634 | 32.634 | 32.634 | 1.741 | 34.374 |
| Mole Flow, kmol/s | 0.040 | 0.040 | 0.040 | 0.040 | 0.040 | 0.749 | 0.749 | 0.749 | 0.040 | 0.789 |
| Mole Fractions (wet basis) | | | | | | | | | | |
| $CO_2$ | 0.93224 | 0.93224 | 0.93224 | 0.93224 | 0.93224 | 0.9615 | 0.9615 | 0.9615 | 0.93224 | 0.96 |
| $H_2O$ | 2.7E-07 | 2.7E-07 | 2.7E-07 | 2.7E-07 | 2.7E-07 | 1.1E-06 | 1.1E-06 | 1.1E-06 | 2.7E-07 | 1E-06 |
| $N_2$ | 0.01079 | 0.01079 | 0.01079 | 0.01079 | 0.01079 | 0.0063 | 0.0063 | 0.0063 | 0.01079 | 0.00653 |
| $O_2$ | 0.04242 | 0.04242 | 0.04242 | 0.04242 | 0.04242 | 0.02358 | 0.02358 | 0.02358 | 0.04242 | 0.02454 |
| Ar | 0.01455 | 0.01455 | 0.01455 | 0.01455 | 0.01455 | 0.00862 | 0.00862 | 0.00862 | 0.01455 | 0.00893 |

Table A - 3. Conditions of the main streams for Base Case #201 – High purity, Coal, base case.

| | 1 | 4 | 7 | 8 | 9 | 10 | 11 | 12 | 13 | 14 | 15 | 16 | 17 |
|---|---|---|---|---|---|---|---|---|---|---|---|---|---|
| Temperature, °C | 60.00 | 30.79 | 28.00 | 28.00 | 27.88 | -3.37 | -13.08 | -49.82 | -49.82 | -24.78 | -27.06 | -14.07 | -14.07 |
| Pressure, bar(a) | 0.93 | 15.01 | 29.45 | 28.45 | 28.45 | 27.88 | 27.32 | 26.78 | 26.78 | 26.24 | 23.25 | 23.25 | 23.25 |
| Mass Vapor Fraction, - | 1.000 | 1.000 | 1.000 | 1.000 | 1.000 | 1.000 | 0.911 | 0.062 | 0.000 | 0.067 | 0.086 | 0.000 | 0.000 |

| Mass Density, kg/m$^3$ | 1.4 | 27.8 | 60.4 | 58.0 | 57.1 | 67.7 | 77.2 | 537.1 | 1125.8 | 508.7 | 415.4 | 1001.4 | 1001.4 |
|---|---|---|---|---|---|---|---|---|---|---|---|---|---|
| Mass Flow, kg/s | 37.046 | 35.185 | 39.090 | 35.142 | 40.378 | 40.378 | 40.378 | 40.378 | 37.503 | 37.503 | 37.503 | 32.267 | 27.137 |
| Mole Flow, kmol/s | 0.916 | 0.813 | 0.903 | 0.810 | 0.938 | 0.938 | 0.938 | 0.938 | 0.861 | 0.861 | 0.861 | 0.733 | 0.617 |
| Mole Fractions (wet basis) | | | | | | | | | | | | | |
| $CO_2$ | 0.83254 | 0.93837 | 0.9386 | 0.9411 | 0.91184 | 0.91184 | 0.91184 | 0.91184 | 0.95936 | 0.95936 | 0.95936 | 0.99999 | 0.99999 |
| $H_2O$ | 0.11536 | 0.00291 | 0.00266 | 1E-06 | 8.7E-07 | 8.7E-07 | 8.7E-07 | 8.7E-07 | 9.4E-07 | 9.4E-07 | 9.4E-07 | 1.1E-06 | 1.1E-06 |
| $N_2$ | 0.00902 | 0.01017 | 0.01017 | 0.0102 | 0.01404 | 0.01404 | 0.01404 | 0.01404 | 0.00571 | 0.00571 | 0.00571 | 8.2E-08 | 8.2E-08 |
| $O_2$ | 0.03096 | 0.0349 | 0.0349 | 0.035 | 0.05497 | 0.05497 | 0.05497 | 0.05497 | 0.02697 | 0.02697 | 0.02697 | 9.7E-06 | 9.7E-06 |
| Ar | 0.01212 | 0.01366 | 0.01366 | 0.0137 | 0.01914 | 0.01914 | 0.01914 | 0.01914 | 0.00796 | 0.00796 | 0.00796 | 2.2E-07 | 2.2E-07 |

| | **18** | **19** | **20** | **21** | **23** | **24** | **26** | **27** | **28** | **29** | **30** | **31** | **CO2-110** |
|---|---|---|---|---|---|---|---|---|---|---|---|---|---|
| Temperature, °C | -23.68 | -14.07 | -50.86 | 21.84 | 28.00 | 21.84 | -49.82 | 20.00 | -26.73 | 0.00 | 21.10 | 28.00 | 28.00 |
| Pressure, bar(a) | 17.27 | 23.25 | 6.45 | 6.32 | 17.02 | 16.92 | 26.78 | 26.24 | 23.15 | 22.68 | 29.03 | 28.45 | 110.00 |
| Mass Vapor Fraction, - | 0.072 | 0.000 | 0.218 | 1.000 | 1.000 | 1.000 | 0.868 | 1.000 | 1.000 | 1.000 | 1.000 | 1.000 | 0.000 |
| Mass Density, kg/m$^3$ | 400.4 | 1001.4 | 73.4 | 11.8 | 33.0 | 33.8 | 68.7 | 42.5 | 55.8 | 46.4 | 55.1 | 52.1 | 668.4 |
| Mass Flow, kg/s | 27.137 | 5.131 | 5.131 | 5.131 | 5.131 | 27.137 | 2.875 | 2.875 | 5.235 | 5.235 | 5.235 | 5.235 | 32.267 |
| Mole Flow, kmol/s | 0.617 | 0.117 | 0.117 | 0.117 | 0.117 | 0.617 | 0.077 | 0.077 | 0.128 | 0.128 | 0.128 | 0.128 | 0.733 |
| Mole Fractions (wet basis) | | | | | | | | | | | | | |
| $CO_2$ | 0.99999 | 0.99999 | 0.99999 | 0.99999 | 0.99999 | 0.99999 | 0.38109 | 0.38109 | 0.72612 | 0.72612 | 0.72612 | 0.72613 | 0.99999 |
| $H_2O$ | 1.1E-06 | 1.1E-06 | 1.1E-06 | 1.1E-06 | 1.1E-06 | 1.1E-06 | 1.1E-07 | 1.1E-07 | 3.1E-08 | 3.1E-08 | 3.1E-08 | 3.1E-08 | 1.1E-06 |
| $N_2$ | 8.2E-08 | 8.2E-08 | 8.2E-08 | 8.2E-08 | 8.2E-08 | 8.2E-08 | 0.10717 | 0.10717 | 0.03847 | 0.03847 | 0.03847 | 0.03846 | 8.2E-08 |
| $O_2$ | 9.7E-06 | 9.7E-06 | 9.7E-06 | 9.7E-06 | 9.7E-06 | 9.7E-06 | 0.36775 | 0.36775 | 0.18172 | 0.18172 | 0.18172 | 0.18172 | 9.7E-06 |
| Ar | 2.2E-07 | 2.2E-07 | 2.2E-07 | 2.2E-07 | 2.2E-07 | 2.2E-07 | 0.144 | 0.144 | 0.05369 | 0.05369 | 0.05369 | 0.05369 | 2.2E-07 |